# CFD SIMULATION OF SURGE AND SWAB PRESURES IN CONCENTRIC AND ECCENTRIC ANNULI USING POWER-LAW FLUID.

by

Husiyandi A/L Husni

14793

Dissertation submitted in partial fulfilment of

the requirements for the

Bachelor of Engineering (Hons)

(Petroleum)

JANUARY 2015

**Universiti Teknologi PETRONAS**
*Bandar Seri Iskandar,*
*31750 Tronoh,*
*Perak Darul Ridzuan,*
*Malaysia*

# CERTIFICATION OF APPROVAL

**CFD SIMULATION OF SURGE AND SWAB PRESURES IN CONCENTRIC AND ECCENTRIC ANNULI USING POWER-LAW FLUID.**

By

Husiyandi A/L Husni

A project dissertation submitted to the

Petroleum Engineering Programme

Universiti Teknologi PETRONAS

In partial fulfilment of the requirement for the

BACHELOR OF ENGINEERING (Hons)

(PETROLEUM)

Approved by

_____

(Mr Titus Ntow Ofei)

Universiti Teknologi PETRONAS

Bandar Seri Iskandar, 31750 Tronoh,

Perak Darul Ridzuan, Malaysia.

# CERTIFICATION OF ORIGINALITY

This is to certify that I am responsible for the work submitted in this project, that the original work is my own except as specified in the references and acknowledgements, and that the original work contained herein have not been undertaken or done by unspecified sources or persons.

_____

Husiyandi A/L Husni

# ABSTRACT

In deepwater exploration, wellbore pressure stability must be maintained to avoid a catastrophic accident such as blowout. Accounting for the factors contributing to wellbore pressure is beneficial to ensuring the stability of the wellbore. In this study, a Computational Fluid Dynamic (CFD) is used to simulate the surge and swab pressure in concentric and eccentric annular geometry using Power-Law fluid. The study fully utilises the CFD software: ANSYS 15.0 and the Fluid Flow (CFX) model to analyse the major factors that affects surge/swab pressure. These include; tripping pipe velocity, wellbore geometry, fluid rheology, pipe eccentricity, flow regime and whether the pipe is closed or open. The model geometries were designed with ANSYS workbench and meshed with tetrahedron elements for concentric annulus and hexahedron elements for eccentric annulus. Grid independent study was performed to compute an optimum mesh size to reduce the computational time to run the simulations. The simulation results are compared with the experimental results both for concentric and eccentric annulus using four (4) different types of test fluids (1.00% PAC-A, 0.75% PAC-A, 1.00% PAC-B, and 0.75% PAC-B). The simulation model was validated against experimental surge pressure data with very good agreement (the highest MPE is 14.3%), thus, confirming the validity of the current model setup. However, the narrow slot model correlation proposed by Crespo et al., under predict the experimental surge pressure of Power-law fluid with the highest mean percentage error (MPE) of 96.9%. Moreover, the degree of eccentricity has substantial effects in the surge and swab pressure. It has been determined that the effect of eccentricity by 0.9 reduced the surge pressure gradient by 18%. Based on the velocity profile analysis, it is observed that as the axial velocity increases, more fluid near the inner pipe boundary is dragged in a downward motion. Furthermore, it is showed that when the inner pipe tripping velocity increases, the yielded plug flow region decreases. According to dynamic viscosity analysis, it is strongly agreed the higher dynamic viscosity relates to the lower sheared velocity in the mid annulus. Moreover, the centre of the annulus generates higher dynamic viscosity and decreases as it approach the inner and outer pipe wall. The study shows how CFD methods can replicate the actual drilling operation especially surge/swab prediction.

# ACKNOWLEDGEMENTS

The author would like to take this opportunity to express his profound gratitude to Universiti Teknologi PETRONAS for providing the platform for the research project to be conducted.

The author also take this opportunity to express a deep sense of gratitude and regards to his supervisor, Mr. Titus Ntow Ofei, Lecturer, Petroleum Engineering, Universiti Teknologi PETRONAS, for his cordial support, valuable information and exemplary guidance, which help the author in completing the final year project. Also, to Dr Tamiru Alemu Lemma, as the Internal Examiner for this project, who giving constructive comments to improve this project.

The author would like to thank Almighty, her parents, brother, sisters and friends for their constant encouragement without which this report would not be possible.

Thank you

# TABLE OF CONTENTS

# LIST OF FIGURE

# LIST OF TABLES

# ABBREVIATIONS AND NOMENCLATURES

| | |
|---|---|
| **CFD** | Computational Fluid Dynamic |
| **PL** | Power-law |
| ***e*** | Eccentricity |
| **MPE** | Mean percentage error |
| **CPU** | Central processing unit |

# CHAPTER 1
# INTRODUCTION

## 1.1 Background of Study

### 1.1.1 Computational Fluid Dynamic (CFD) using ANSYS Workbench 15.0

ANSYS Workbench 15.0 is an engineering simulation software that has the capability to simulate the Computational Fluid Dynamic (CFD) fluid flows in a virtual environment. This is very beneficial in term of cost and time since one doesn't need to go to the real field or setup a costly experiment study to run a simulation of our desired study. Nowadays, ANSYS software is used to solve extreme engineering problems and challenges. Example of simulation that can be run are, but not limited to fluid dynamic of gas turbine engines, vacuum cleaners, mixing vessal and many others engineering backgrounds.

For this study, Fluid Flow (CFX) is used to analyse the surge/swab pressure of Power-Law fluid along the pipe annulus with varying tripping velocity. The simulation is carried out both in concentric and eccentric annular geometries. Then, benchmark study is run where the CFX model is validated with experimental results of the surge pressure for different eccentricities [1]. After both models are validated, parametric study carried out to analyse the effect of eccentricity on surge pressure and the flow pattern of the Power-Law fluid in the pipe annulus.

### 1.1.2 Surge and swab pressure

Past few years and numerous studies were done regarding the surge and swab pressure analysis. Recently, experiment under controlled condition [2] [3] were conducted.

Based on theory and field studies [4] [5], the major factors affecting surge pressure are depend on drillpipe tripping velocity and wellbore geometry. Moreover, other factors that give influence to the surge pressure are fluid rheology, pipe eccentricity, flow regime and whether the pipe is closed or open. Surge pressure gives many problems when the tripping velocity is very high especially in narrow annular clearance. This condition usually happens in deepwater wells with close margin between pore pressure gradient and fracture pressure gradient.

In many drilling operations, the prediction of frictional pressure losses in the wellbore is mostly exclusive of the surge and swab pressures. Surge/swab pressure which is unaccounted for may result in erroneous hydraulics calculations and may lead to downhole problems such as: loss circulation, formation fracture, kick or even blowout.

### 1.1.3 Eccentricity

Based on Schlumberger Oilfield Glossary [6], eccentricity is described as how much offset a pipe is within another pipe or in the open hole and usually expressed in term of percentage (%). If the inner pipe is perfectly centred within the outer pipe, the inner pipe is said to be concentric. And if the inner pipe is lying close to the outer pipe and has an offset from the centre, the inner pipe is considered eccentric. However, if the inner pipe touches or in contact with the wall of outer pipe, the condition is said to be fully eccentric (100 % eccentric).

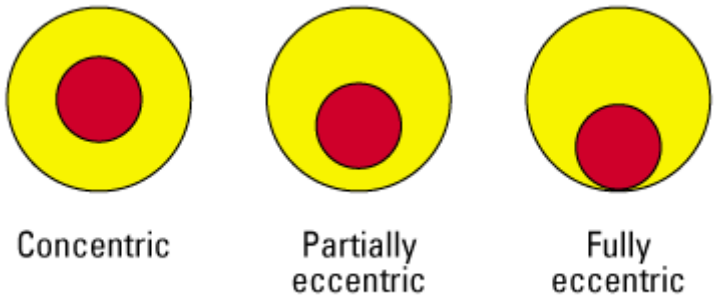


Figure 1-1. Diagram of type of eccentricity. (Modified from [6])

For this study, the eccentricity of the inner pipe would be 0% (concentric) and 90% (partially eccentric). The offset of the inner pipe from centre will be determine by using formula below;

$$e = \frac{2\delta}{d_2 - d_1} \tag{1.1}$$

where,

$$e = \text{eccentricity}$$

$$\delta = d\text{istance of offset from centre}$$

$$d_1 = \text{diameter of the inner pipe}$$

$$d_2 = \text{diameter of the outer pipe}$$

For this study, the geometry of the inner and outer pipe is designed using DesignModeler component in ANSYS Workbench 15.0.

### 1.1.4 Power-Law Fluid Model (Ostwald-de Waele)

This model is used for better representation of the behavior of a drilling fluid since the viscosity is the shear rate dependent. As shear rate increases most of drilling fluid shows a shear thinning behavior. The model is given as [7]:

$$\tau = k\gamma^n \tag{1.2}$$

where

$$\tau = \text{shear stress } \left(Pa \text{ or } \frac{lbf}{100ft^2}\right)$$

$$k = \text{consistency index } \left(Pa - s^n \text{ or } eq.cP \text{ or } \frac{lbf - s^n}{ft^2}\right)$$

$$\gamma = \text{shear rate } \left(\frac{1}{s}\right)$$

$$n = \text{flow behaviour index (dimensionless)}$$

Shear stress is defined as the force per unit area required to move a fluid at a given shear rate. Meanwhile, shear rate is defined as the flow velocity gradient in the direction perpendicular to the flow direction. The higher the shear rate, the higher the friction between the flowing particles. The parameters $k$ and $n$ can be calculated form the measured rheometer data.

$$n = 3.32 \log\left(\frac{R_{600}}{R_{300}}\right) \tag{1.3}$$

$$k = 510\left(\frac{R_{600}}{511^n}\right) \tag{1.4}$$

There are two (2) types of Power-Law fluid which are Dilatant Power-Law and Pseudoplastic Power Law.

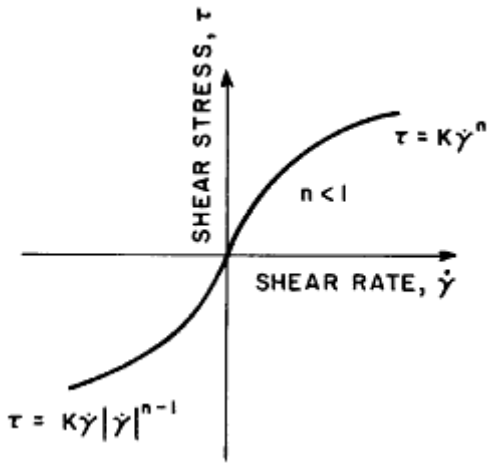


Figure 1-2. Pseudoplastic Power Law, n<1. (Modified from [7])

Pseudoplastic Power Law fluid show a nonlinear shear stress-shear rate relationship and it is also called shear-thinning fluids, i.e, apparent viscosity decreases with increasing shear rate [7]. Polymer solutions are one of the example of Pseudoplastic Power Law fluid.

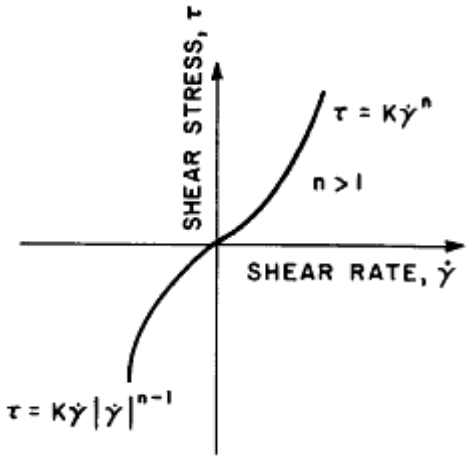


Figure 1-3. Dilatant Power Law, n>1. Modified from [7])

Dilatant Power Law fluid show a nonlinear shear stress-shear rate relationship. Also called shear-thickening fluids, i.e, apparent viscosity increases with increasing shear rate.

For this study, the Power-Law fluid used is 1.00 % and 0.75% concentration of Polyanionic cellulose (PAC) and the data is given in Table 3-3.

## 1.2 Problem Statement

During well drilling, surge and swab pressure generated are very critical in design of drilling hydraulics. Underestimating the surge and swab pressure can bring a fatal effect on the drilling operation especially on the drilling cost. Issues, for example, lost circulation due to fractured formation, fluid influx resulting in kick, breakdown of the formation at casing shoe due to limited kick tolerance or blowout can occur when surge/swab pressure losses are either overestimated or underestimated. Therefore, an accurate surge/swab pressure model is needed to make a prediction of the downhole pressure mainly in the wells with narrow safe pressure windows, in drilling operations such as slimholes, low clearance casing, deepwater and extended-reach well applications. Hence, special emphasis is required to identify the critical limit during tripping, running casing and cementing operations. Failure to identify these pressure variations can cause increase in operation cost and time.

In the past, the prediction of surge and swab pressure have been carried out through the theoretical model and experimental study. Crespo and Ahmed [3] have studied on surge/swab pressure prediction for yield power law fluid in concentric annulus. Moreover, Srivastav et al. [1] have carried out an experimental study on surge/swab pressure in eccentric annulus for Newtonian, Power-Law and Yield Power-Law (Herschel Buckley) fluids. Based on the experiment setup, the test fluid is always static in the annulus which doesn't represent the real condition which it can be both static and circulating. These surge/swab pressure model prediction is considered has limited applications as it ignore the circulating drilling fluid in the annulus. The model prediction can over estimate or under estimate the surge/swab pressure as it ignore one of the vital part in the hydraulic of the wellbore.

To address the above challenges, CFD simulation is adopted to study the effect of pipe tripping velocity and eccentricity on surge/swab pressure in a vertical annular wellbore. In addition, the flow patterns of the fluid under various conditions will be observed.

## 1.3 Objectives

The main objectives of this study are:

i. To analyse the effect of eccentricity and drillpipe tripping velocity on the swab/ surge pressure.
ii. To compare the experimental, empirical and numerical simulation results.
iii. To predict and analyse the velocity flow pattern in the annular geometry.

## 1.4 Scope of Study

This study uses CFX-Fluid Flow as an analysis component. The surge pressure simulation is run in a vertical well. The annular geometry are concentric and eccentric annulus. The test fluid is Power-Law fluid. The flow is single phase, isothermal and steady state fluid flow. The flow regime is considered laminar and fully developed. The inner pipe is close ended and moving axially. The boundary condition are velocity inlet, pressure outlet and no slip wall boundary.

# CHAPTER 2
# LITERATURE REVIEW

## 2.1 Definition of Surge and Swab Pressure

The phenomenon of surge and swab pressure is illustrated in Figure 2-1. During drilling operations, a downward movement of drillpipe causes a pressure increase and it is known as surge pressure. Similarly, the upward movement of the drillpipe causes a pressure decrease and it is known as swab pressure. Figure 2-1 shows the flow pattern of a mud in the annulus as a result of the axial motion of the drillpipe. The surging may increase the hydrostatic pressure of the drilling mud to a point that may exceed the fracture gradient, and a circulation loss of the drilling fluid will occur. In extreme conditions, the drilling fluid that is lost to the formation causes the fluid level to drop. This causes drop in the hydrostatic pressure of the drilling mud, hence, allows the formation fluid to enter the wellbore. As the fluid influx into the wellbore, kick and blowout can occur.

However, upward movement of drillpipe may create a hollow space at the bottom of drillpipe and the swab pressure created by this action also causes formation fluid influx into the wellbore. This is because of the hollow space decreases the hydrostatic pressure of the drilling fluid. In extreme conditions, swab and surge pressure lead to blowout of the well. In addition, alternating pressure change between surge and swab pressure can cause hole sloughing, or other borehole issue, such as solids deposited at the bottom of the borehole. For that reason, prediction of accurate surge and swab pressure is a pre-requisite for efficient drilling operation [8].

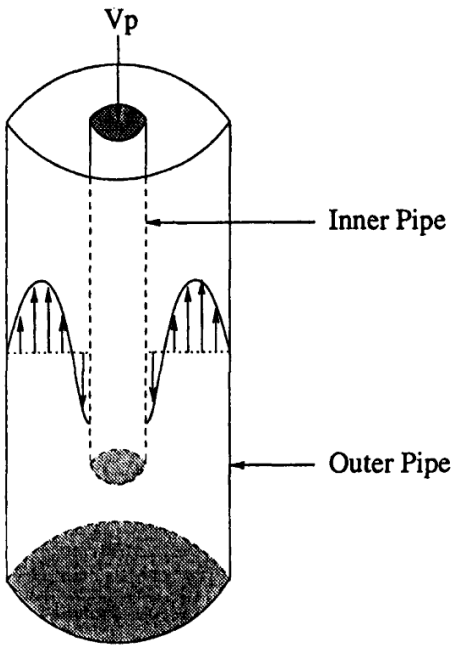


Figure 2-1. Flow due to axial motion of the inner pipe. (Modified from [9])

## 2.2 Effect of Pipe Velocity

Few studies [4] [8] have analysed the effect of drilling fluid properties and drilling parameters on surge/swab pressure. The major parameters involve are the drillpipe tripping speed and wellbore geometry. Other parameter are flow regime, fluid rheology and whether the pipe is open or closed [2] [3]. However, tripping speed is largely dependent on the diameter ratio between the drillpipe and borehole.

Recently, based on the experimental study conducted, the diameter ratio, tripping speed and fluid yield stress can cause an extreme increase in surge pressure [3]. High diameter ratio (small annular clearance) makes the pressure variation very sensitive to the changing of the drillpipe tripping velocity. This is because, the increase in drillpipe diameter causes an increase in volume of mud displaced and simultaneously the flow rate in the annular increases. Increase of flow rate also causes the surge pressure to increase. The effects of diameter ratio and trip velocity on surge pressure is illustrated in Figure 2-2.

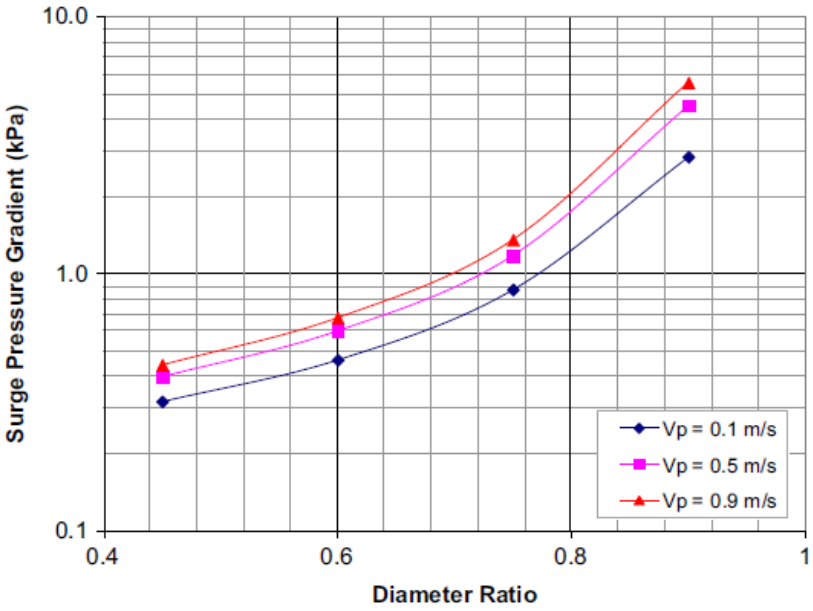


Figure 2-2. Surge pressure gradient as a function of diameter ratio (Modified from [3] )

Moreover, the surge pressure has a slight impact from a high yield stress with increasing drillpipe velocity. When the yield stress is high, the fluid becomes more shear thinning. The decrease in apparent viscosity with increasing shear rate makes the surge pressure become less affected to the increase in drillpipe velocity [3]. Figure 2-3 presents the influence of drillpipe velocity on surge pressure at constant yield stress of mud.

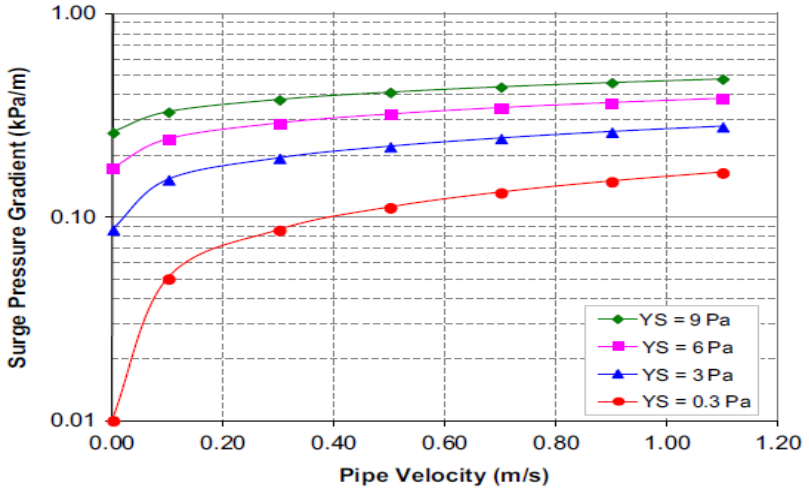


Figure 2-3.Surge pressure gradient vs. trip speed for fluid with different yield stress (Modified from [3])

The most crucial parameter to determine the surge/swab pressure is the pressure gradient that causes the flow [9]. When the pressure gradient is identified, the pressure gradient is multiplied with the distance of the location to obtain the surge/swab pressure at a certain point of interest. Surge and swab pressures have the same magnitude but different direction. Therefore, surge pressure from inner pipe movement of downward direction will be analysed in this study.

### 2.3 Effect of Eccentricity

Based on experimental study by Crespo and Ahmed [3], for a vertical well with eccentric drillpipe, the surge pressures is reduced by 42% compared to a concentric position as shown in Figure 2-4. The pressure gradient is decreasing when increase in drillpipe eccentricity in the borehole. Proper and correct model of eccentricity can help in determining the critical drillpipe tripping velocity and hence can reduce the drilling time and cost.

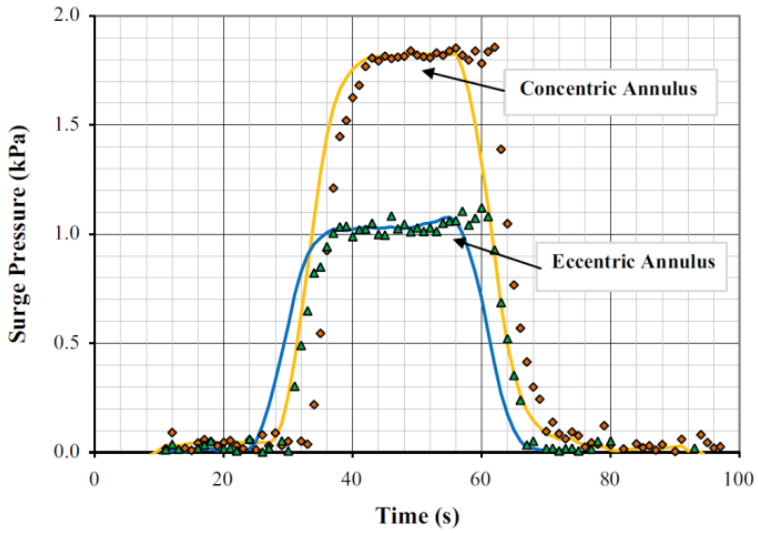


Figure 2-4. Measured surge pressures at different annular eccentricities (Modified from [3])

In horizontal and inclined well configuration, the inner pipe lie down on the low side of the borehole. The main factor that need to be analysed for optimizing the tripping speed are the thickness of the cuttings and the eccentricity of the drillpipe. Eccentricity is acknowledged to have a major effect on annular pressure losses [10]. The drillpipe become eccentric because of the gravity during directional drilling of horizontal and inclined wells. A study from Zamora and Jefferson [11] shows that the tendency of cutting to settle down and build up at the bottom side of the borehole increases rapidly when the inclination of the drillpipe is greater than about

10° from the vertical. According to Hussain and Sharif [9], the higher the eccentricity, the lower the pressure gradient (surge pressure), however, for partially blocked eccentric annulus, the pressure gradient is found to decrease with an increase in the blockage height [9]. Figure 2-5 depicts a partially blocked horizontal annular wellbore.

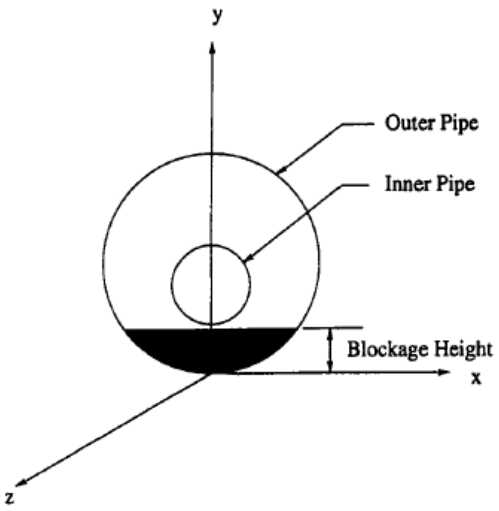


Figure 2-5. Coordinate system and flow geometry (Modified from [9])

Ignoring the pressure reducing effect of eccentricity on surge and swabs pressure may eventually lead to underestimating the tripping speeds, and thereby increase non-productive time and operation costs.

Based on numerical study of Hussain and Sharif [9], the surge/swab pressure is reduced considerably by 35% in eccentric annulus compared to concentric annulus.

# CHAPTER 3

# METHODOLOGY

## 3.1 CFD simulation Flow Chart

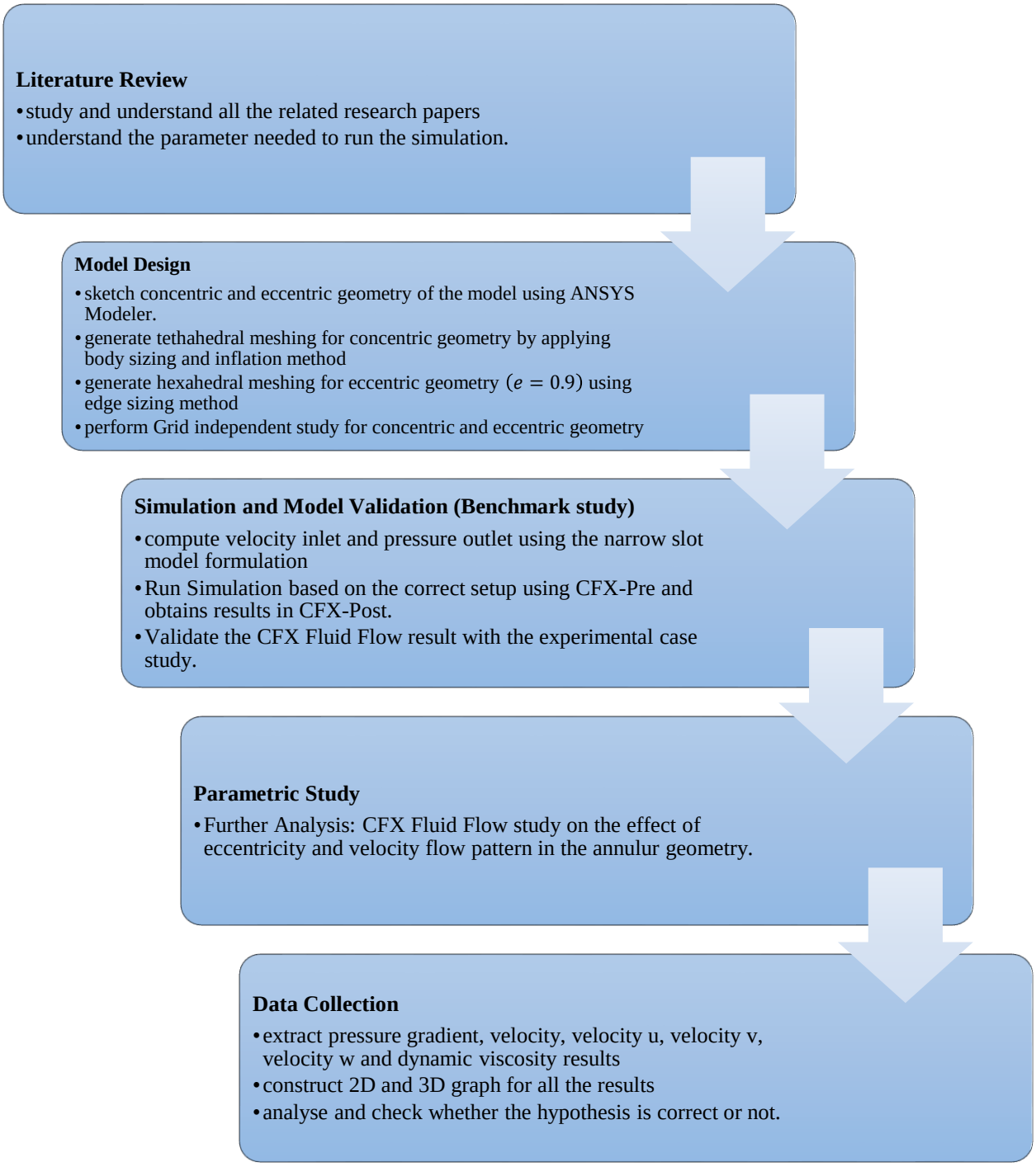


Figure 3-1. CFD simulation flow chart.

## 3.2 Numerical simulation model

A single phase component of Power Law (PL) fluid flowing through concentric and eccentric annuli is numerically simulated using the Computational Fluid Dynamics (CFD) software, ANSYS-CFX 15.0. The simulation is using a CFX-Fluid flow as the analysis component to sketch the geometry, performed meshing, running the model validation and parametric study. The software packages is divided into (a) DesignModeler: sketching geometries (b) CFX-Mesh: for meshing the geometry into smaller grids (c) CFX-Pre: to setup the input data and all parameters including fluid parameters, initial parameter and boundary conditions (d) CFX-Solver: for solving the partial differential flow equations and CFX-Post: to generates output of the simulations. The CFX-Solver is assumed to generate a very good results when the solution is converged to a root mean square (RMS) of normalised residual error reached below $10^{-5}$. The inner pipe is moving axially with variation of tripping velocity ($0.1\,^{ft}/_{s}$ to $0.8\,^{ft}/_{s}$) while the outer pipe is remain stationary. The carrier fluid obey the rheology of Power-Law fluid (Polyanionic Cellulose). Prediction of surge pressure gradient as a function of drillpipe tripping velocity, eccentricity and rheological models are analysed and results are presented in Chapter 4. In addition, contours of axial flow profiles and dynamic viscosity are also presented. The simulation were run on a personal computer with the following specification: Windows 8 64-bit operating system, with 8 GB RAM and Intel i5-2500K processor at 3.3 GHz. The study was planned and conducted based on the project Gant Chart presented in APPENDIX D.

### 3.2.1 Governing equation

In this study, the Power-law fluid in the annulus is modelled based on following assumptions: (a) the fluid is single phase, incompressible and isothermal, and (b) the flow regime is considered laminar, steady state and fully developed. The governing conservation equations for mass (3.1), momentum (3.2), and a passive scalar (3.3), expressed in Cartesian coordinates are as follows:

$$\frac{\partial \rho}{\partial t} + \frac{\partial}{\partial x_j} \cdot \left(\rho U_j\right) = 0 \tag{3.1}$$

$$\frac{\partial}{\partial t}(\rho U_i) + \frac{\partial}{\partial x_j} \cdot \left(\rho U_j U_i\right) = -\frac{\partial \mathrm{P}}{\partial x_i} + \frac{\partial}{\partial x_j}\left(\mu_{eff}\left(\frac{\partial U_i}{\partial x_j} + \frac{\partial U_j}{\partial x_i}\right)\right) \tag{3.2}$$

$$\frac{\partial}{\partial t}(\rho\varphi) + \frac{\partial}{\partial x_j} \cdot (\rho U_j \varphi) = \frac{\partial}{\partial x_j}\left(\Gamma_{eff}\left(\frac{\partial \varphi}{\partial x_j}\right)\right) + S_\varphi \tag{3.3}$$

In ANSYS-CFX, the governing sets of partial equations were discretized using a finite volume method, which first involves discretizing the spatial domain using a mesh. According to Ofei et al. [12], the discretized governing equations, along with the initial and boundary conditions are solved for each finite volume in ANSYS-CFX solver.

### 3.2.2 Physical model and carrier fluid

The inner pipe and outer pipe are vertical. The inner pipe is close ended and moving axially. The annular geometry is modelled with two different eccentricity$(e)$ which are $e = 0$, for concentric annulus and $e = 0.9$, for eccentric annulus. The annulus is bounded by an outer and inner pipe diameter, $OD$ and $ID$ respectively; the origin of which is located either at the centre or off-centred from the outer cylinder with an offset margin, $\delta$ as shown in Figure 3-4 and Figure 3-7. The outer pipe represents the actual borehole and the inner pipe represents the actual drill pipe. Experimental test parameters are adopted in the CFD simulation to demonstrate the real fluid flow behaviour in the annular geometry. Table 3-1 below shows the vertical test section parameters for experimental setup. The concentric and eccentric geometry are drawn exactly based on the experimental setup. To analyse the flow pattern, the axial measurement in concentric geometry is taken along sector A-A (Figure 3-4). For eccentric geometry, the axial measurement is taken along sector B-B and C-C to represent the 'narrow region' and 'wide region' of the geometry (Figure 3-7).

Table 3-1. Experimental Vertical Test Section Parameter [1]

| Parameter | Value |
|---|---|
| Outer Pipe Diameter $(OD, inch)$ | 2.00 |
| Inner Pipe Diameter $(ID, inch)$ | 1.32 |
| Pipe eccentricity $(e)$ | 0.9 |
| Length of pipe $(L, inch\ [ft])$ | 148 [12.33] |

The vertical test section parameters are illustrates in the figures below (Figure 3-2 and Figure 3-3)

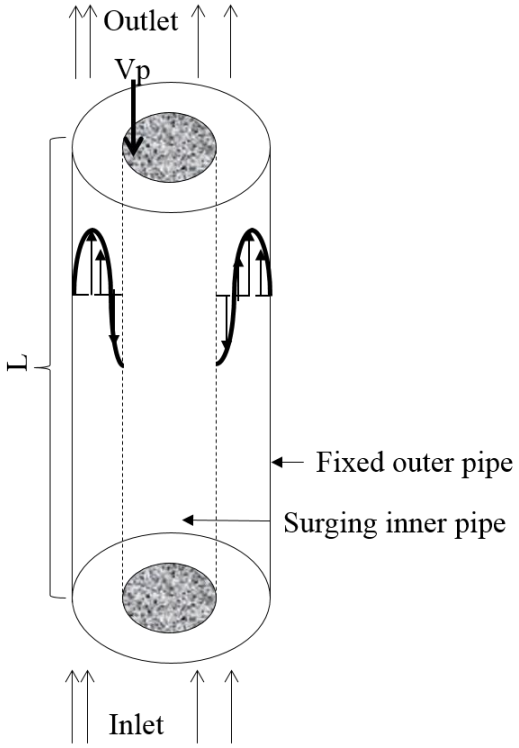


Figure 3-2. Physical flow model (concentric).

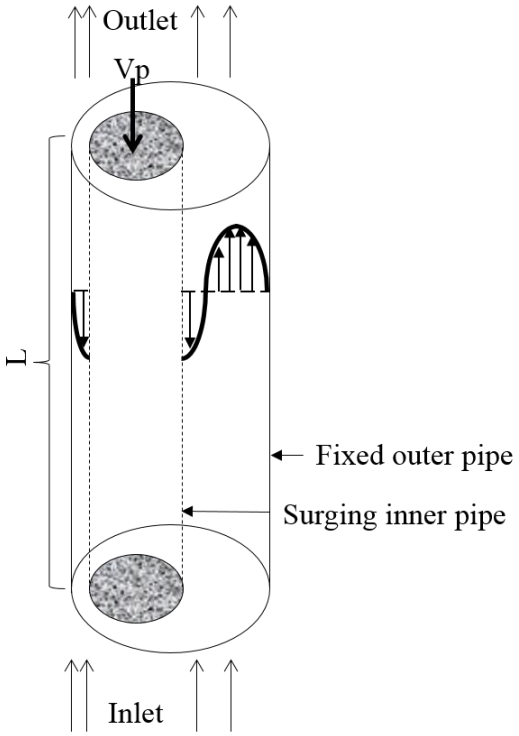


Figure 3-3. Physical flow model (eccentric)

### 3.2.2.1 Concentric annulus geometry

For concentric geometry, the eccentricity, $e = 0$. Hence, the centre of circle for inner pipe and outer pipe is the same.

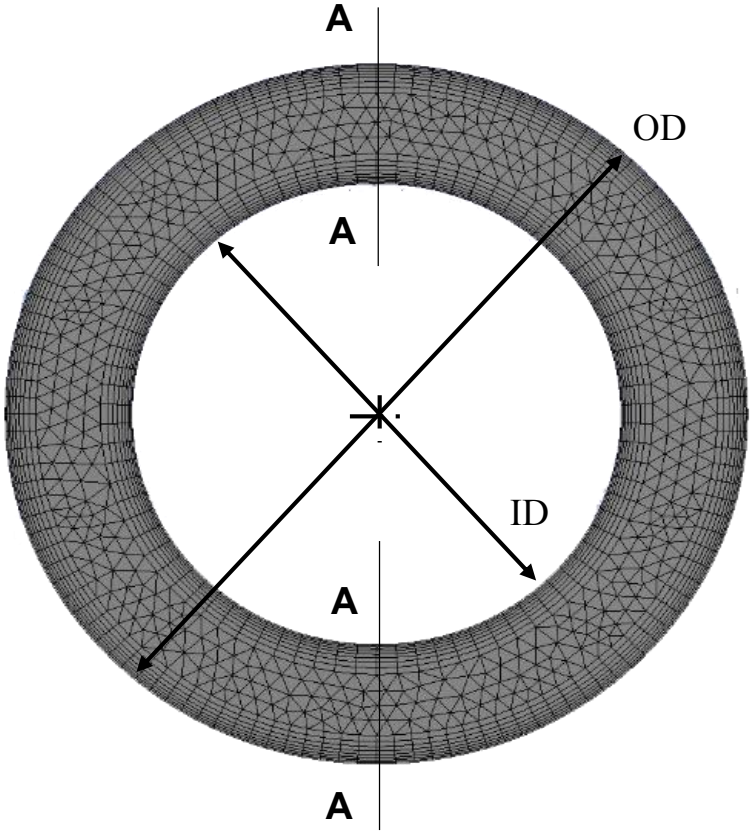


Figure 3-4. Concentric annulus without applying symmetry (2D).

Figure 3-5. Concentric annulus without applying symmetry (3D).

To reduce computational times, symmetry is applied to the concentric geometry. In this way, the number of elements can be reduced from $1.68E+06$ to $0.8E+06$ but still maintaining the result's accuracy and consistency. After applying symmetry option, the computational time reduced from 2.238E+03 seconds to 8.551E+02 seconds.

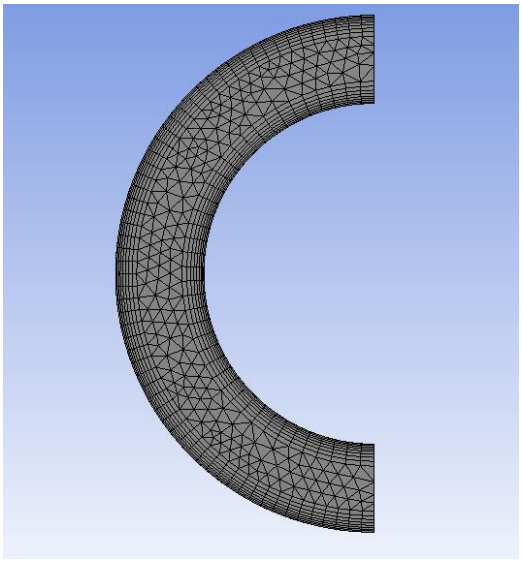

Figure 3-6. Concentric annulus with symmetry applied.

#### 3.2.2.2 Eccentric annulus geometry

Calculation is needed in sketching the eccentric model using equation 1.1 in page 2 (Eccentricity). From the calculation, for eccentric annular geometry, the centre of inner pipe is 0.306 inch away from the origin of outer pipe.

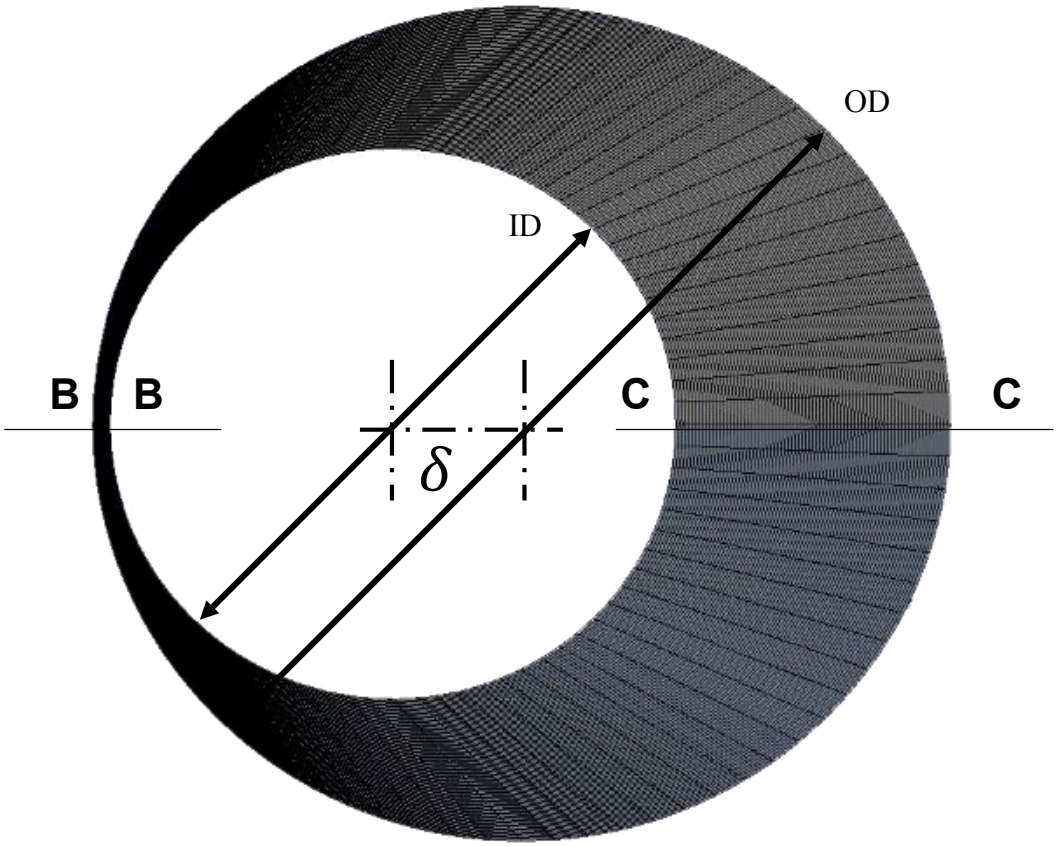


Figure 3-7. Eccentric annulus geometry (2D).

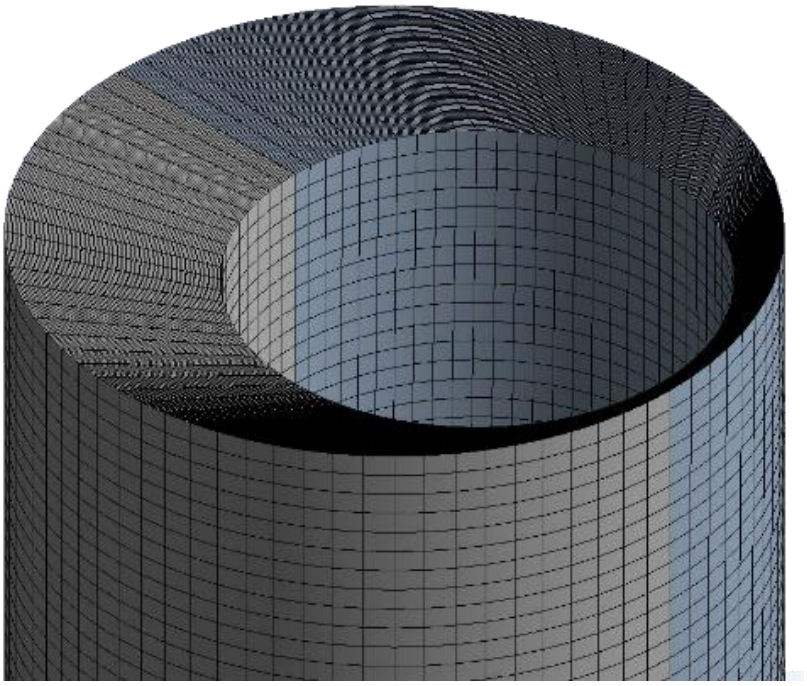

Figure 3-8. Eccentric annulus geometry (3D).

#### 3.2.2.3 Hydrodynamic entrance length

The pipe configuration in the experiment setup is 148 inch. However, this is considered too long in numerical simulation and thus, more computational time is needed as more number of element for a longer pipe length. Therefore, to optimise the computational time and at the same time to ensure a fully developed flow with the end effect of the pipe is eliminated, a hydrodynamic length for four different type of fluids must be calculated.

According to Shook and Roco [13], for a fully developed Newtonian fluid flow to occur in a pipe, the pipe length $L$, must be longer than the hydrodynamic entrance length $L_h$, which presented as;

$$L_h = 0.062 N_{Re}(D) \tag{3.4}$$

Where,

$$N_{Re} = \text{Reynolds number.}$$

However, for a single phase flow in annular gap with non-Newtonian fluid, such expression as in Equation (3.4) does not yet exist in the literature. As a rule of thumb, the author has adopted Equation (3.4) by replacing the pipe diameter, $D$ with an outer pipe diameter, $OD$.

For a shear-thinning non-Newtonian fluid, the fully developed velocity distribution is flatter than for a Newtonian fluid. The constant in Equation (3.4) decreases for more shear thinning fluids [14]. The entrance length for a shear thinning fluid is therefore lower than that estimated using Equation (3.4). A study from Rohsenow et al. [14] reports the values of 0.0575, 0.048, and 0.034 for $n$ = 1, 0.75, and 0.5, respectively. Therefore, the author assumed that the combine effect if axial velocity of the inner pipe and annular geometry of the pipes would influence the flow Reynolds number, thus, the constant in Equation (3.4) is accepted for estimating the hydrodynamic length of annular flow. Since the entrance length is proportional to the flow Reynolds number, a substantial pipe length may be required as the Reynolds number increases. As a result, the pipe length must be chosen so as to satisfy the entrance length condition for the case with the highest Reynolds number. Therefore, hydrodynamic entrance length must be calculated for all four types of fluids as each fluid has different flow behaviour index $(n)$ and

fluid consistency index ($K$). Table 3-2 below shows the hydrodynamic length, $L_h$ for all four types of fluids.

Table 3-2. Hydrodynamic entrance length for all fluids.

| Fluids | 1.00% PAC-A | 0.75% PAC-A | 1.00% PAC-B | 0.75% PAC-B |
|---|---|---|---|---|
| $N_{Re}$ | 17.65 | 38.85 | 15.17 | 30.96 |
| $L_h, ft$ | 0.18 | 0.40 | 0.16 | 0.32 |

Based on the results, the maximum hydrodynamic length, $L_h$ is 0.4 $ft$ for 0.75% PAC-A. Therefore, the pressure gradient in the CFD simulation is measured from 0.5 $ft$ to 0.7 $ft$. Moreover, the length of pipe in the experiment is not adopted into the CFD simulation geometry and the author decides to choose a pipe length of 1.0 $ft$. The reasons are because the length of pipe, 1.0 $ft$ is longer than the maximum hydrodynamic entrance length of 0.4 $ft$ which sufficient enough to ensure fully developed flow and also reduce the CFD computational time.

#### 3.2.2.4 Experimental model Power-Law fluid parameter

Experimental data for Power Law fluid flowing in concentric and eccentric annulus are adopted from Srivastaz [1] and inputted into the CFD simulation model. The fluids are composed of varying concentrations (0.75% and 1.00%) of Polyanionic Cellulose (PAC) based polymeric fluids. The flow behaviour of the PAC based polymeric fluid best fit the power law model. Moreover, the script A with the fluid is used for concentric annulus fluid and B for the eccentric annulus fluid. Table 3-3 below shows the test fluids parameter for concentric and eccentric annular geometry.

Table 3-3. Power-Law Fluid Model Parameter [1]

| Annular Geometry | Concentric | | Eccentric | |
|---|---|---|---|---|
| **Test fluids** | **1.00 % PAC-A** | **0.75 % PAC-A** | **1.00 % PAC-B** | **0.75 % PAC-B** |
| **Temperature (**°F) | 61 | 65 | 59 | 68 |

| | | | | |
|---|---|---|---|---|
| **Yield stress** $(\boldsymbol{\tau_y}, \frac{\boldsymbol{lbf}}{\boldsymbol{100\ ft^2}})$ | 0 | 0 | 0 | 0 |
| **Consistency index** $(\boldsymbol{K}, \frac{\boldsymbol{lbf.s^n}}{\boldsymbol{100\ ft^2}})$ | 2.188 | 0.532 | 2.78 | 0.83 |
| **Flow behaviour index** $(\boldsymbol{n})$ | 0.652 | 0.781 | 0.634 | 0.736 |

### 3.2.3 Boundary condition and meshing

At the inlet, normal speed is specified with stationary mesh motion. The normal speeds at the inlet are varied depending on the inner pipe tripping velocity. At the outlet, a zero opening pressure is specified normal to boundary. The inner pipe and outer pipe is imposed with no slip boundary condition for the fluid flow. The inner pipe (drillpipe) is surging downward with velocity ranging 0.1 $^{ft}/_{s}$ to 0.8 $^{ft}/_{s}$ and the outer pipe (borehole) remain stationary.

For concentric annulus, the 3D geometry is meshed into unstructured tetrahedral elements with inflation layers resulting in approximately $4.45E+05$ to $7.54E+06$ elements generated with element mesh size ranging between $0.03\ inch$ to $0.08\ inch$. In the near-wall region, an inflation layer is created to capture the flow effect at that region. The inflation layer is generated with a first aspect ratio of 10 and maximum layer of 8. The relative thickness of adjacent inflation layer is 1.2 which adopted from default geometric expansion factor. Inflation layer is created near the wall region because the boundary layer affect the velocity gradient as it increases when the velocity is normal to the wall. This required elements at the region to have a high first aspect ratio for efficient meshing. As the tetrahedral mesh is used, a fine surface mesh is required to avoid generating highly distorted tetrahedral elements at the surface. This problem is overcome by the generation of inflation layer that are generated using prism elements to create a finely resolved mesh normal to the wall. In this CFD simulation, inflation layer covers 20% of the inner and outer pipe radii to capture the flow effect of the annular flow as shown in Figure 3-4. The unstructured tetrahedral mesh generate a very good mesh quality as it generates 0.1381 skewness and face angle ranging from 63.501 degree to 125.92 degree.

Excellent mesh quality has a skewness close to 0 and face angle between 10 degree and 170 degree.

However, for eccentric annulus, hexahedral elements type is adopted since the eccentricity is very close to 1. The narrow gap of the eccentric geometry causes the repeated refinement of the unstructured tetrahedral anisotropic subdivision to lead into poor mesh quality. Poor mesh quality is defined as a grid deficiency that leads to an inaccurate flow field solution. Poor meshes can have disparate element sizes, large face angles, high vertex degrees and close to 1 skewness. In this case, the eccentricity if the inner pipe that causes a narrow region in the annulus leads to an inefficient distribution of grid points in the final mesh. Therefore, hexahedral meshes is preferred as it can be subdivided anisotropically in any of the three directions and yield child elements whose face angles are similar to their parents. This ability to anisotropically refine the mesh makes a tremendous difference in the final problem size when directional flow features are present. Moreover, hexahedral meshed also have an advantage in that they yield more accurate fluid flow solutions than their tetrahedral counterparts for the same number of elements. Aftosmis et al. [15] have shown that, in general, tetrahedral elements require approximately double the storage and CPU time than hexahedral tessellations of the same vertices. This is due to the fact that tetrahedral meshes have more edges. These additional edges, however, do not contribute significantly to an improvement in solution accuracy. The hexahedral mesh generates approximately $1.60E+05$ to $2.50E+06$ elements depending on the number of division using edge sizing. It also generates average of 0.4141 skewness and face angle ranging between 90 degree and 154.436 degree. Both mesh quality indicates an excellent mesh quality.

Grid independence studies were conducted on the meshed geometries to optimise the element size until the results are independent to the element size. For concentric annulus, the element size is ranging between $0.03\ inch$ to $0.08\ inch$. For eccentric annulus, the base number of division of the edge sizing are 40, 20 and 100 for radius edge $(r)$, circumference edge $(\theta)$ and length edge $(z)$ (refer APPENDIX A). Then, the base case number of division is multiplied by $1.50, 2.00, 2.25$ and $2.50$ to generate a constant no. of division.

In running the grid independence study, the carrier fluid used for concentric annuli is 1.00% PAC-A while for the eccentric annuli the carrier fluid is 1.00 PAC-B. The inner pipe tripping velocity is $0.8\ \frac{ft}{s}$ for both of the annular geometries with same velocity inlet boundary and pressure outlet boundary. In Figure 3-10, element size $0.05\ inch$ and above show no significant changes in pressure gradient. Therefore, an optimum element size of $0.05\ inch$ with number of elements of $1.68E+06$ is chosen for concentric annular geometry. In Figure 3-11, double $(x2.00)$ multiplication of edge sizing and above shows the pressure gradient is no longer dependent on the element size. Therefore, an optimum number of division for eccentric annulus is two times greater than the base case number of division with hexahedron elements of $1.28E+06$. The hexahedral division are as follow: $80(r) \times 40(\theta) \times 200(z)$ and illustrated in figure below (Figure 3-9).

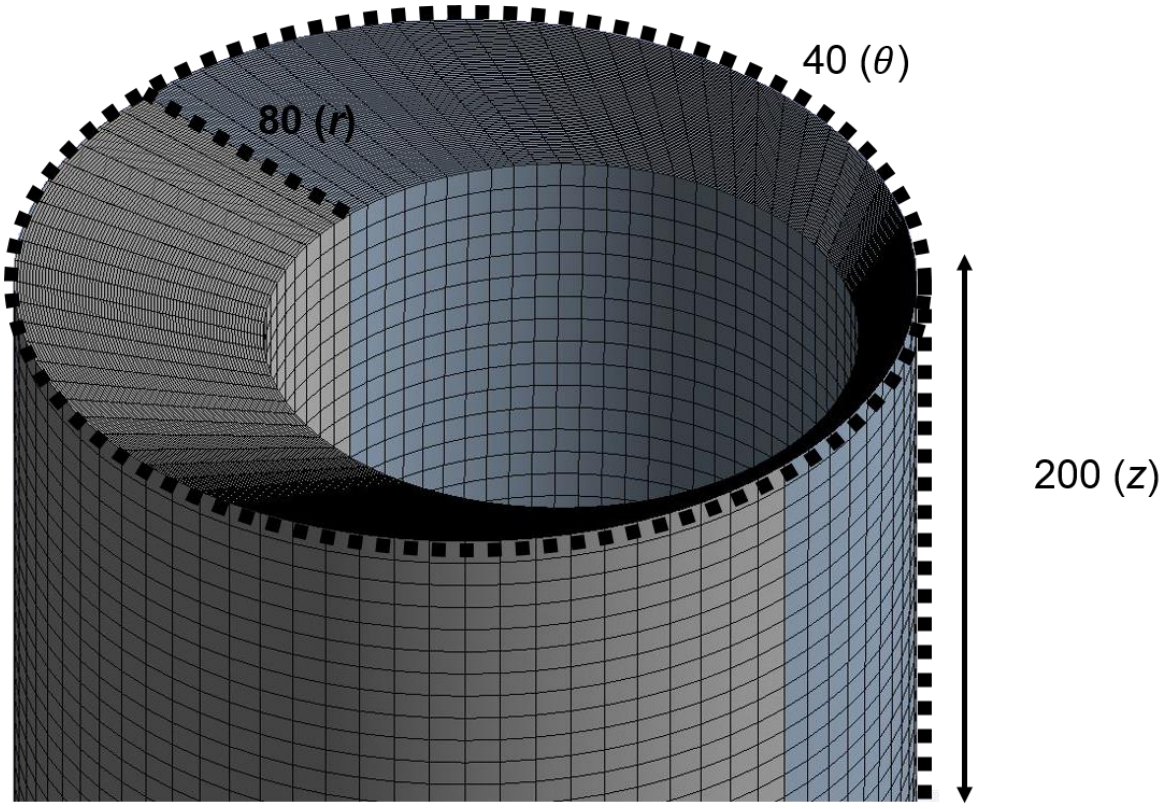


Figure 3-9. Hexahedral meshing

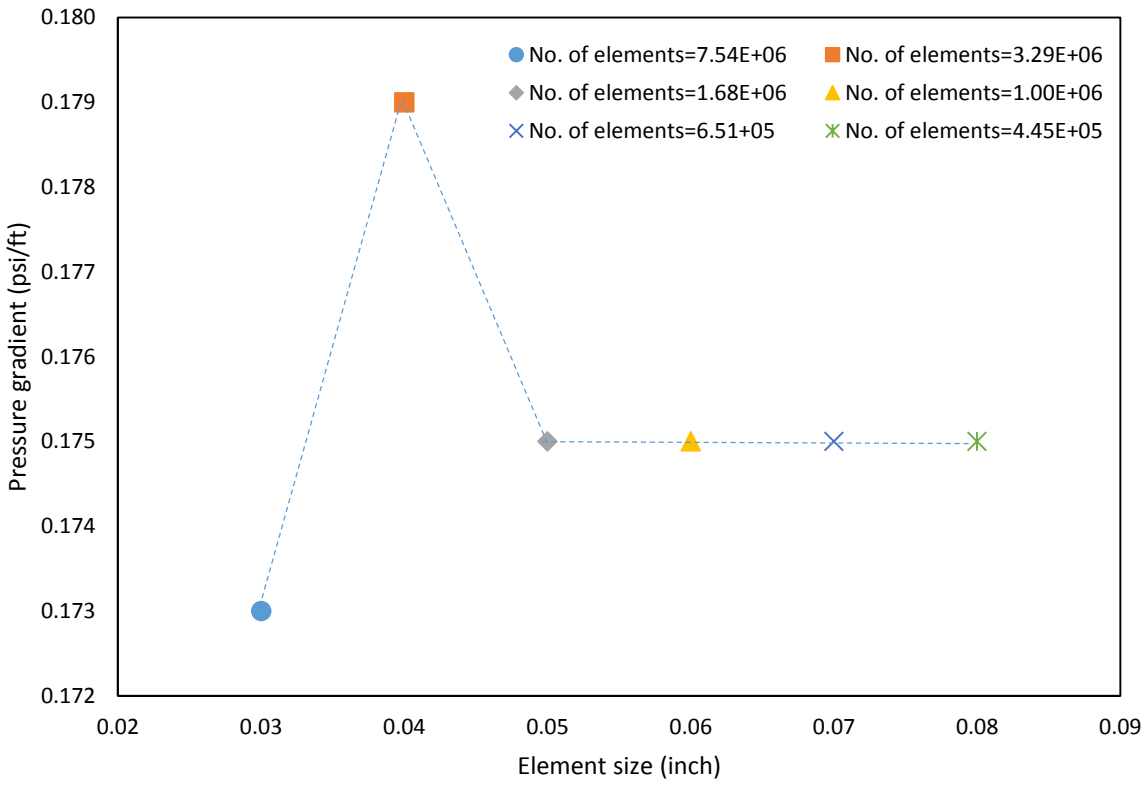


Figure 3-10. Grid independence study for concentric annulus.

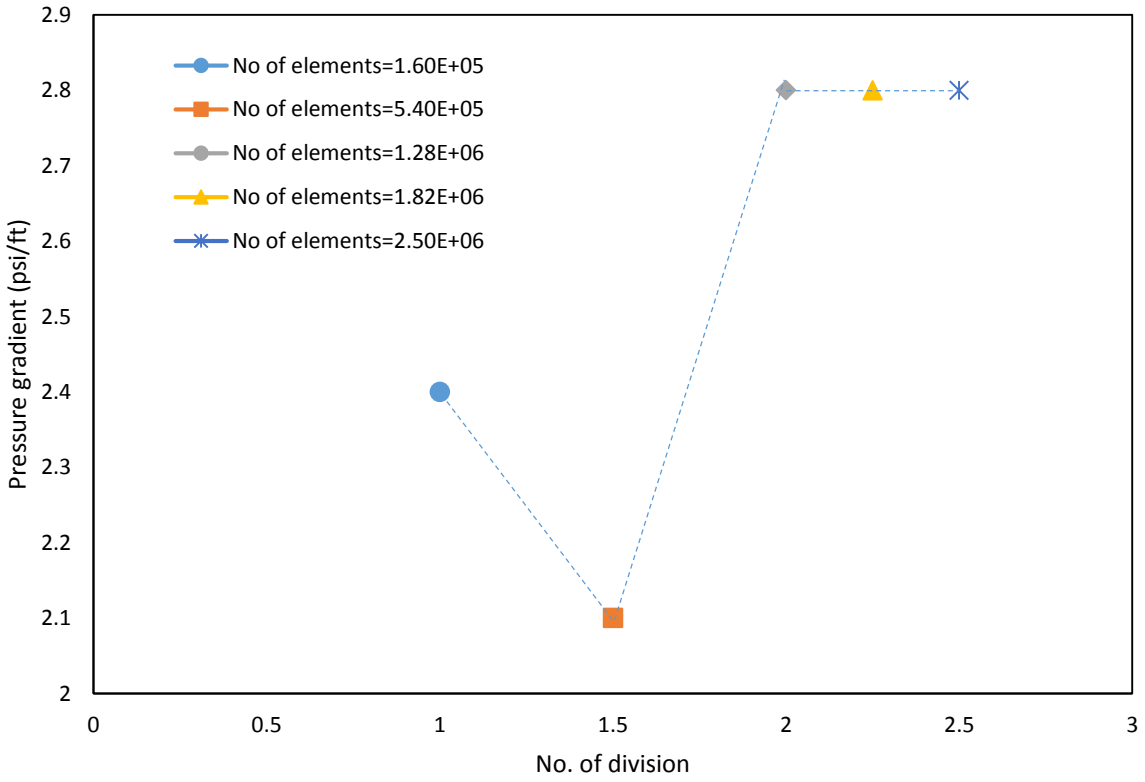


Figure 3-11. Grid independence study for eccentric annulus.

# CHAPTER 4
# RESULTS AND DISCUSSION

## 4.1 Validation of CFD simulations

CFD simulation is validated with the experimental results from [1] for all four types of fluids. CFD simulation is run with inner pipe tripping velocity ranging from 0.1 $^{ft}/_{s}$ to 0.8 $^{ft}/_{s}$ with increment of 0.1 $^{ft}/_{s}$.

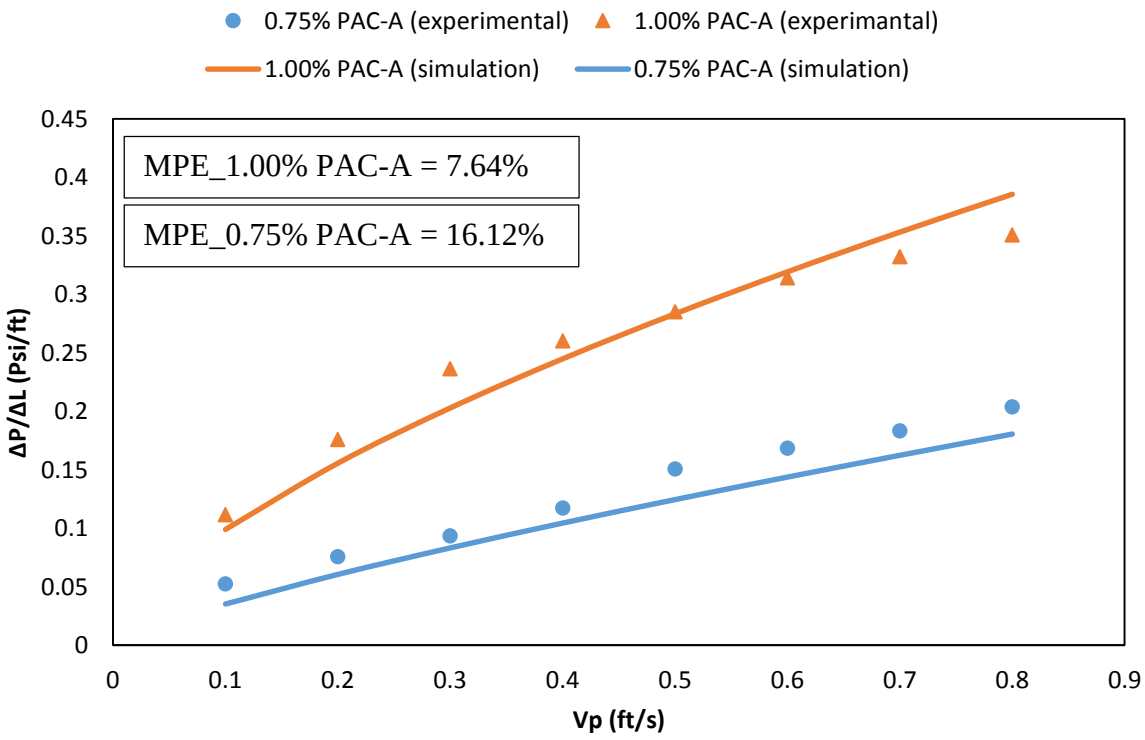


Figure 4-1. Model validation of concentric annulus with experimental results.

In Figure 4-1, for 0.75% PAC-A fluid, the CFD simulations under-predict the experimental results satisfactorily with mean percentage error of 16.12% corresponding inner pipe tripping velocity from 0.1 $\frac{ft}{s}$ to 0.8 $\frac{ft}{s}$. Whereas for 1.00% PAC-A fluid, the CFD simulations shows good agreement where it under-predict the experimental results with the mean percentage error is 7.64%.

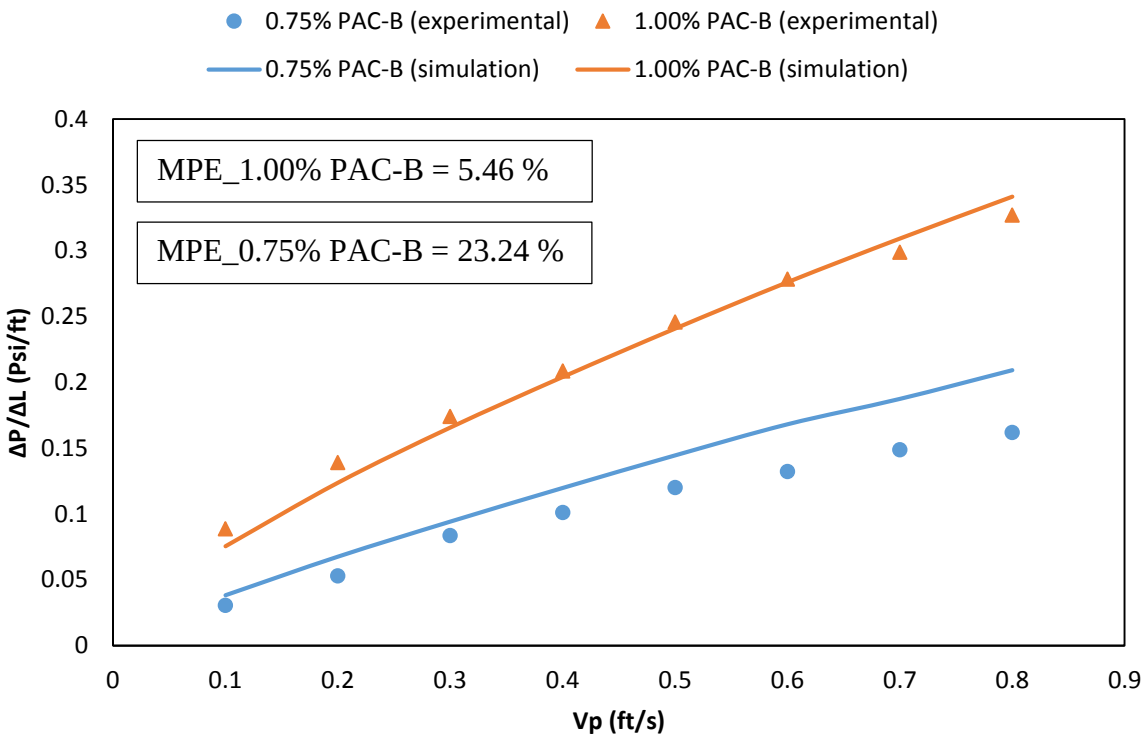


Figure 4-2. Model validation of eccentric annulus with experimental results.

In Figure 4-2, for 0.75% PAC-B fluid, the CFD simulation compared satisfactorily by over-predicting the experimental results with mean percentage error of 23.24%. However for 1.00% PAC-B fluid, the CFD simulation nearly predict the experimental data accurately with mean percentage error is 5.46%.

Based on the results obtained, it shows that the higher the inner pipe tripping velocity, the higher the surge pressure gradient. This strongly agreed with the experimental study done by Srivastav [1], thus, confirming the validity of the CFD simulation model, along with promising low mean percentage error. Tabulated results of the model validation for all fluids is presented in APPENDIX B.

## 4.2 Parametric study

Parametric study was performed mainly to study the effect of eccentricity on surge pressure gradient corresponding to the inner pipe tripping velocity. The axial flow pattern and dynamic viscosity profile in annular geometry are also analysed. Moreover, comparison of CFD, experimental and correlation results are also performed.

### 4.2.1 Comparison of surge pressure calculation using correlation and pressure crossplot

Narrow slot approximation model from Crespo and Ahmed [3] is adopted to compare with the CFD and experimental results. In this section, the analytical correlation and CFD simulations results are compared based on the eccentricity itself. The results of comparison are as follow:

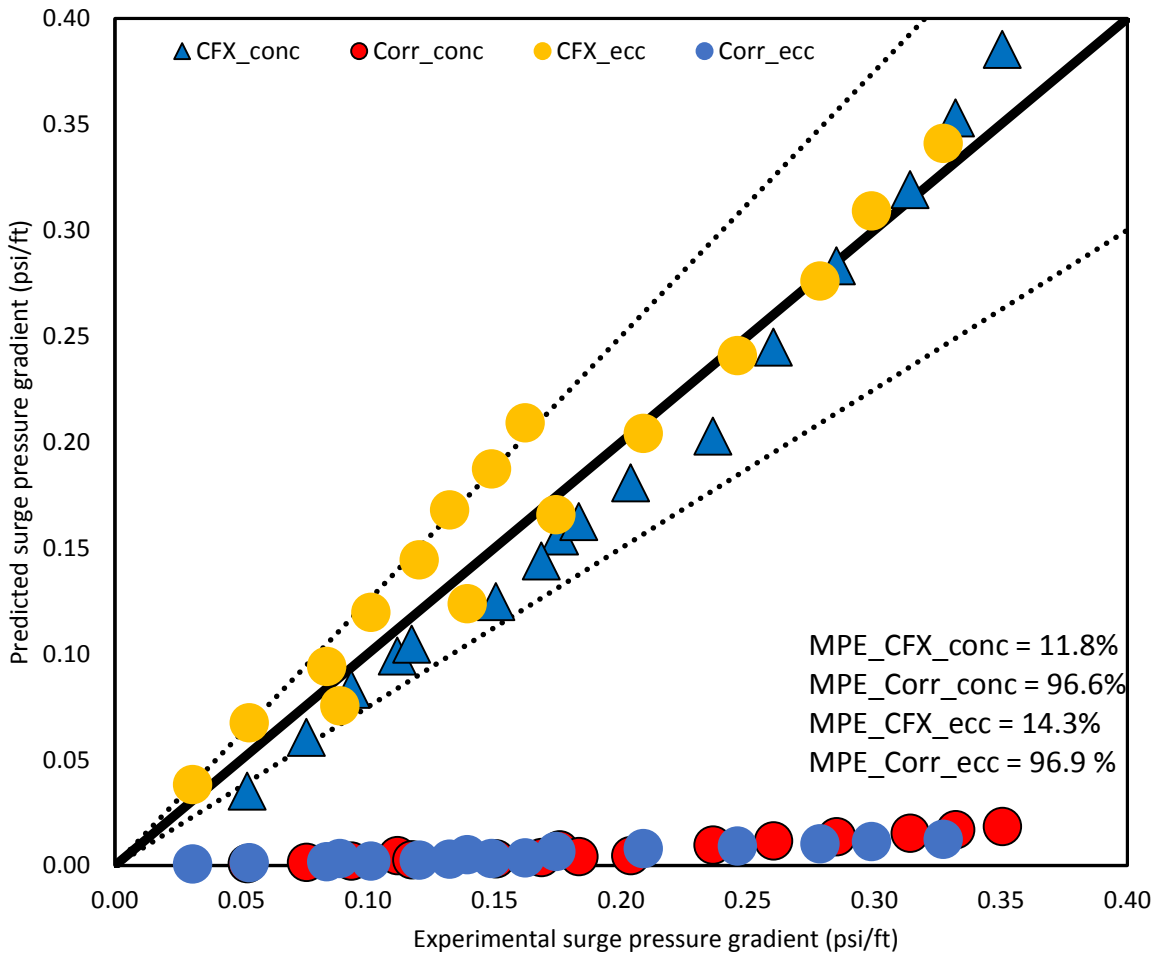


Figure 4-3. Surge pressure crossplot of CFD, experimenatal and correlation results

From the crossplot, it shows that the narrow slot approximation model totally under predict the CFD and experimental results for Power-law fluid. The analytical correlation generates mean percentage error of 96.6% for concentric annulus and 96.9% for eccentric annulus. On the other hand, the CFX results show reliable prediction of surge pressure in comparison with the experimental results as it generates mean percentage error of 11.8% for concentric annulus and 14.3% for eccentric annulus.

### 4.2.2 Effect of eccentricity

To study the effect of eccentricity, 1.00% PAC-A fluid for concentric annulus and 1.00% PAC-B for eccentric annulus from CFD simulation results are selected for comparison.

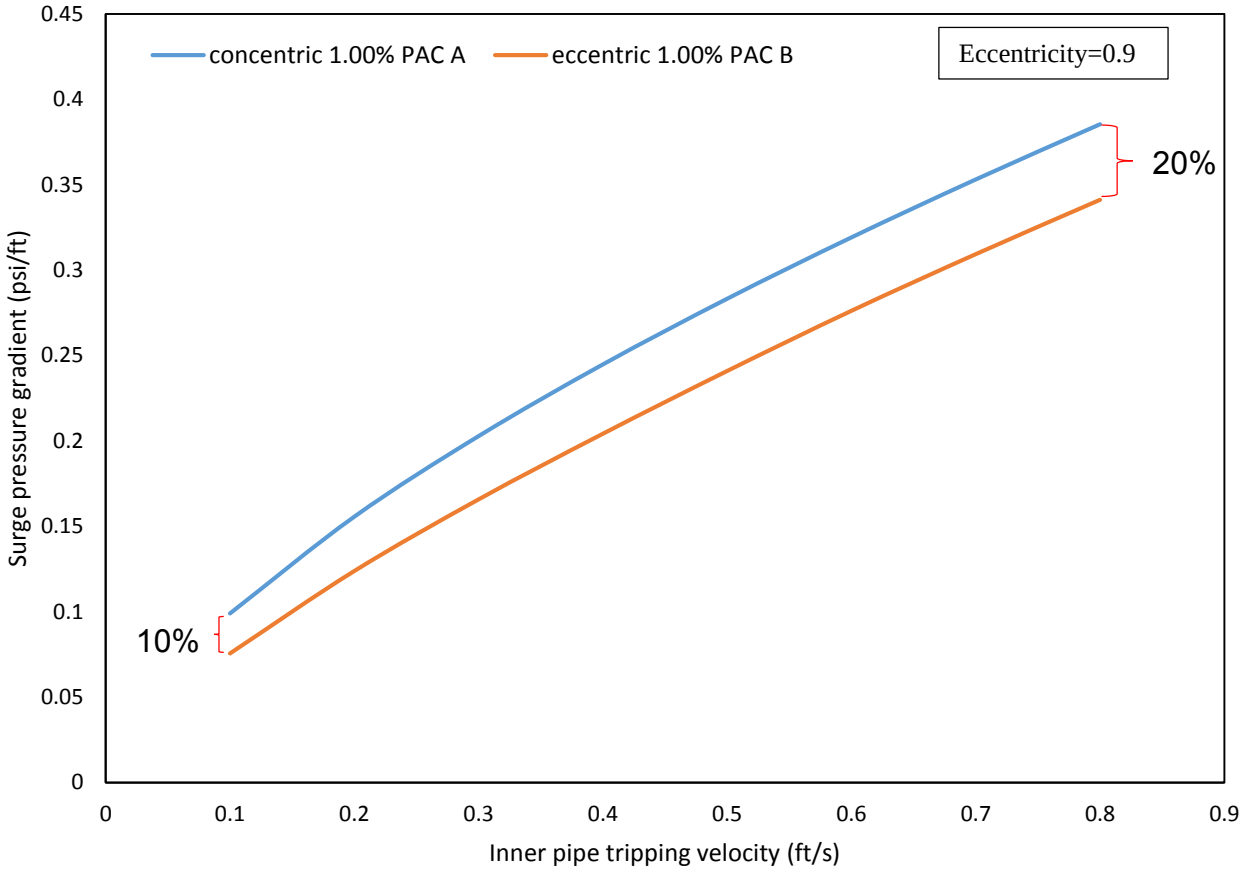


Figure 4-4. Effect of eccentricity on surge pressure gradient.

Figure 4-4 shows that the difference in surge pressure gradient between concentric annulus and eccentric annulus. As similar observation was made by Hussain and Sharif [9], the surge pressure gradient decreases with increasing eccentricity. Based on the calculation, eccentricity of 0.9 reduces the surge pressure gradient by 18%. Moreover, it is observed that as the inner pipe tripping velocity increases, the effect of eccentricity becomes more dominant. It shows that the reduction of surge pressure gradient increases from 10% to 20% as the inner pipe tripping velocity increases. The tabulated results are presented in APPENDIX C.

### 4.2.3 Axial flow pattern.

By CFD simulation, axial flow pattern is analysed in concentric and eccentric annular geometry for all four types of fluids. The flow patterns are plotted along sector A-A for concentric annulus and along sector B-B and C-C for eccentric annulus (see Figure 4-5 to Figure 4-12).

The eccentricity certainly affect the flow pattern in the annular geometry. It is observed that there is no difference in axial velocity profile of fluid 0.75% PAC-A and 1.00% PAC-A in concentric annulus. However, the axial flow profile shows that as the inner pipe velocity increases, more fluid near the inner pipe wall is dragged downward. Hence, the axial velocity profile of the fluid is highest at the central region of the annulus and decreases at the near inner and outer pipe boundary. Moreover, it is also observed that as the inner pipe tripping velocity increases, the axial velocity gradient increases.

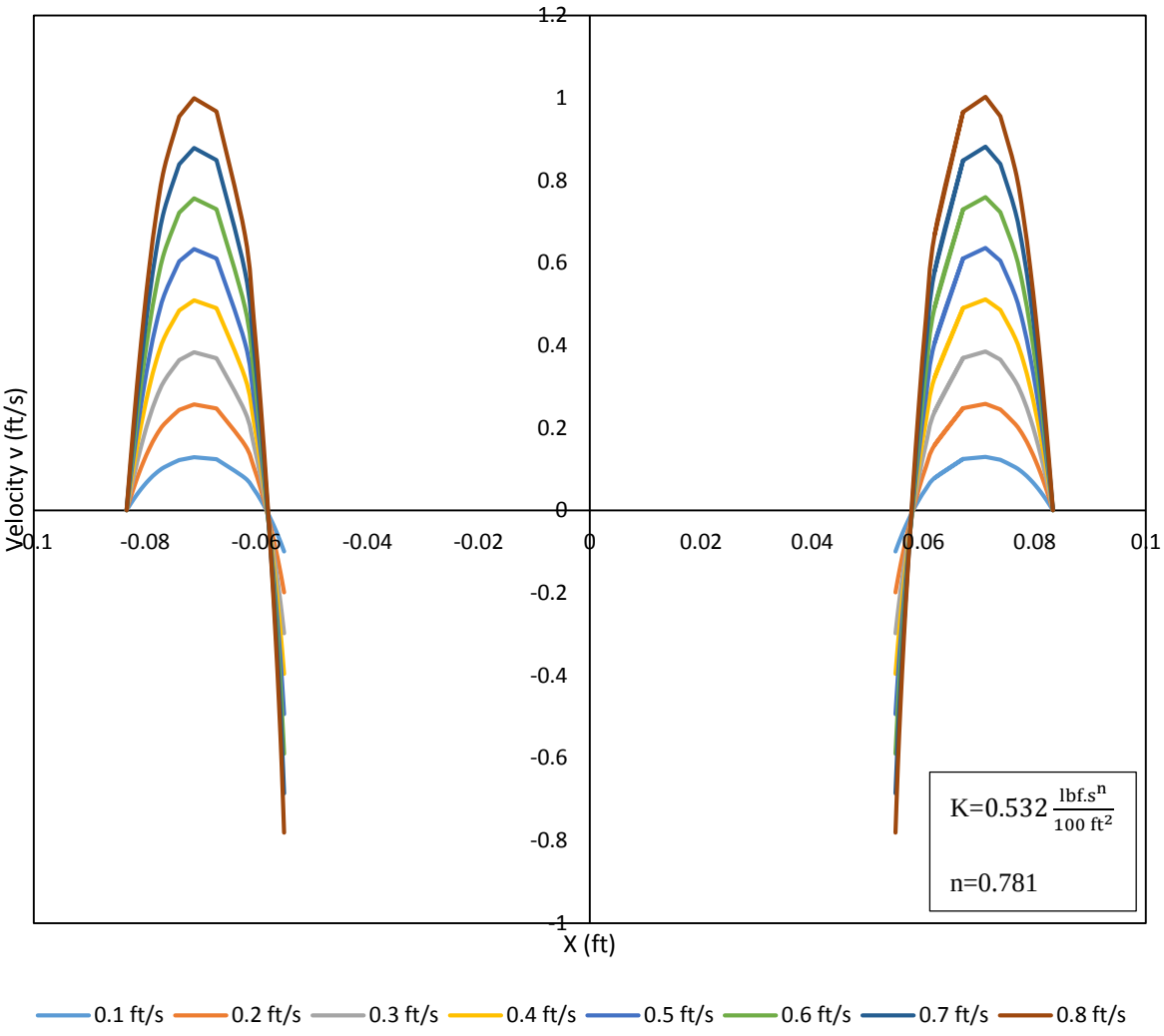


Figure 4-5. Velocity profile concentric 0.75% PAC A (2D)

v=0.8 ft/s

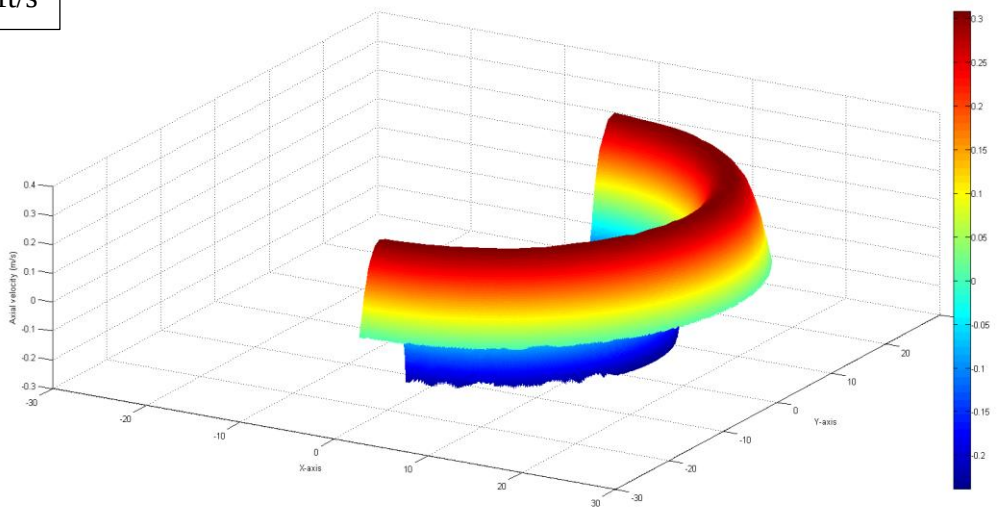


Figure 4-6. Velocity profile concentric 0.75% PAC A (3D)

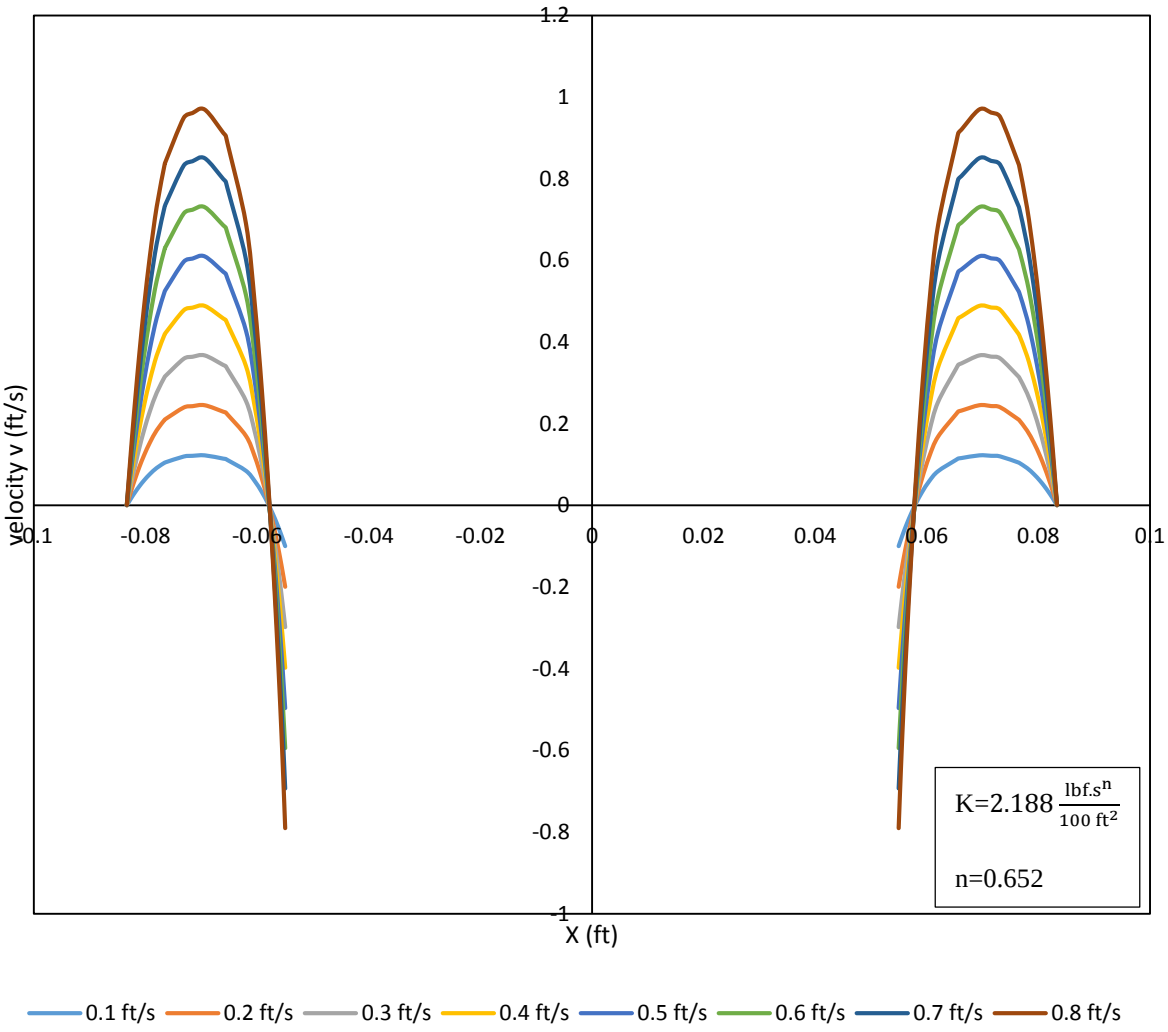


Figure 4-7. Velocity profile concentric 1.00% PAC A (2D)

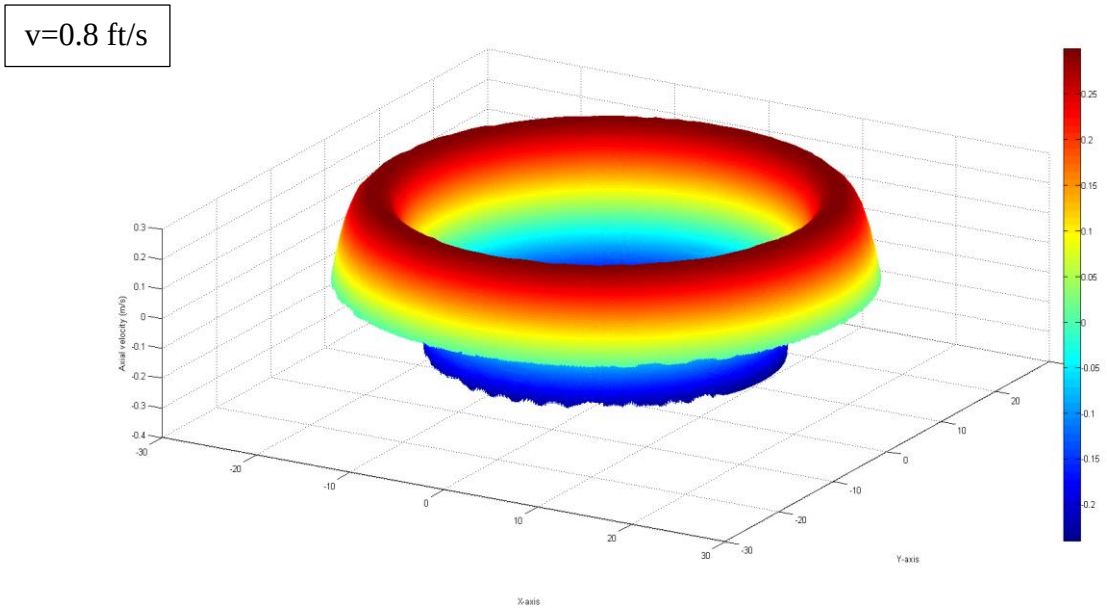


Figure 4-8. Velocity profile concentric 1.00% PAC A (3D)

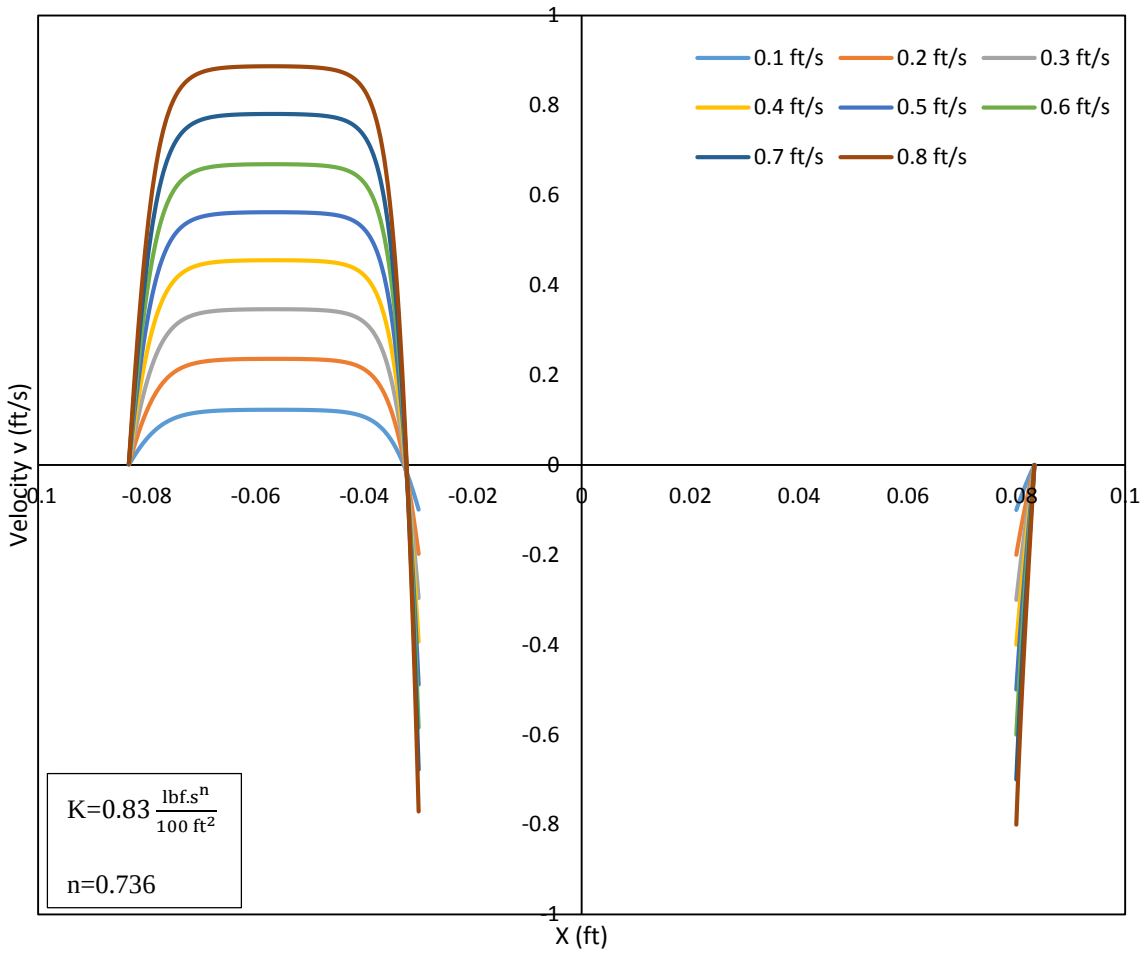


Figure 4-9. Velocity profile eccentric 0.75% PAC B (2D)

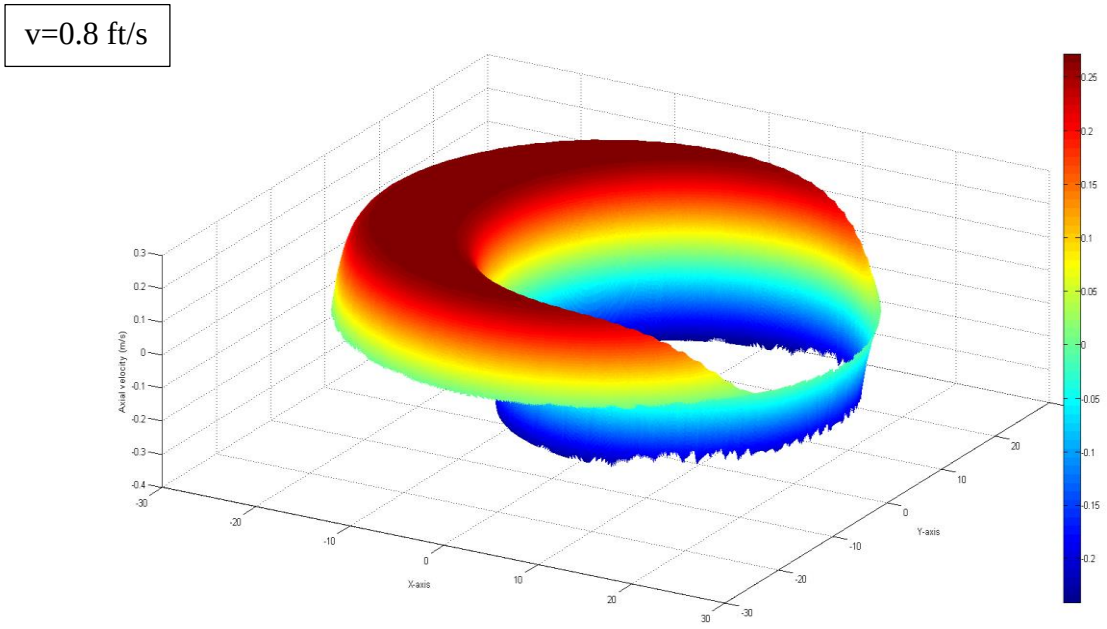


Figure 4-10. Velocity profile eccentric 0.75% PAC B (3D)

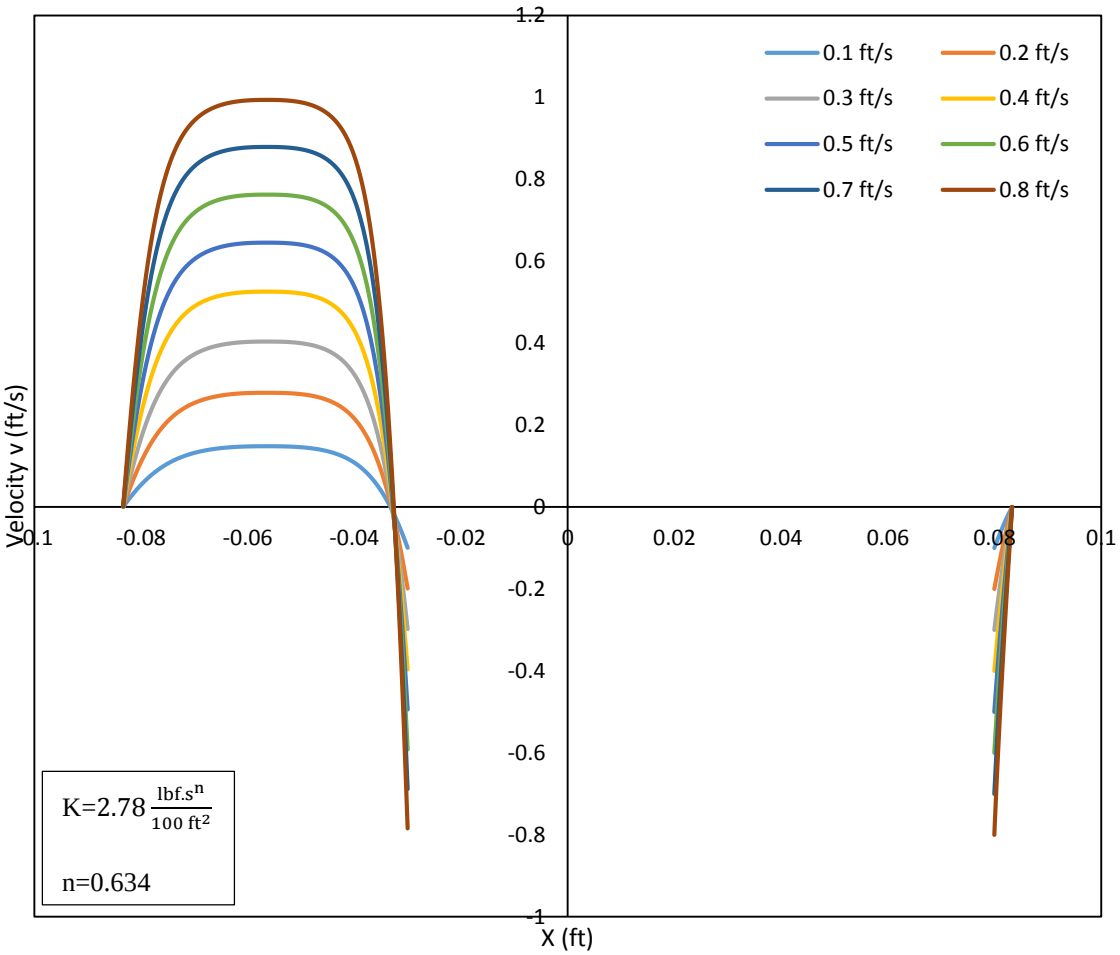


Figure 4-11. Velocity profile eccentric 1.00% PAC B (2D)

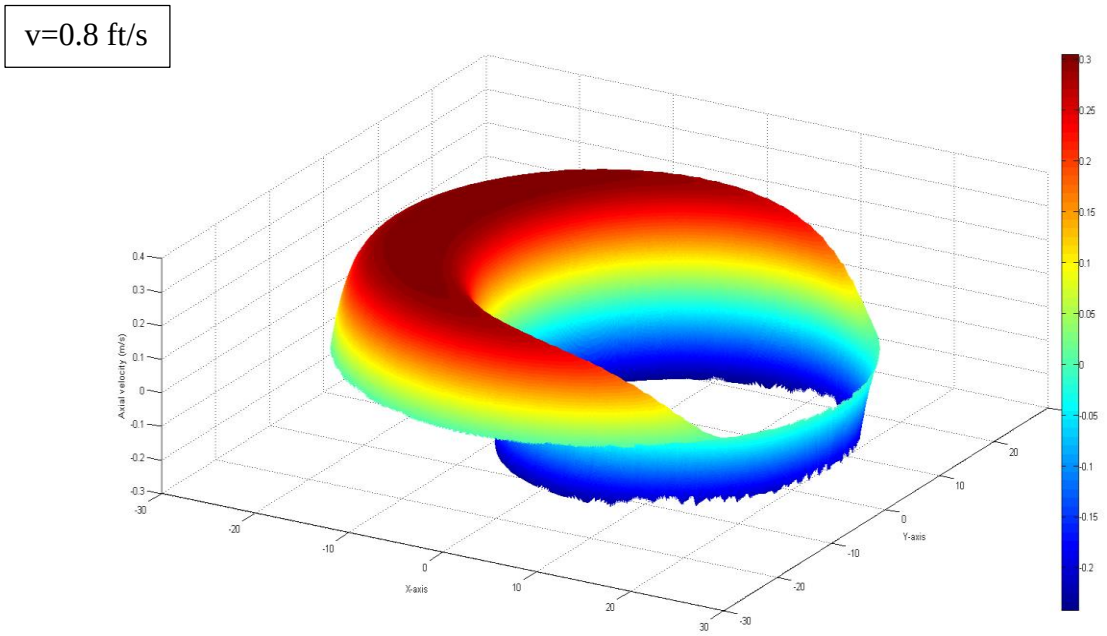


Figure 4-12. Velocity profile eccentric 1.00% PAC B (3D)

In eccentric annulus, the axial velocity profile distribution is measured along the sector B-B for narrow region and sector C-C for the wide region. Along sector B-B, it is observed there is almost no fluid flow in the region. This is because of the combine effect of pipe eccentricity and the dynamic viscosity itself in such that when downward motion of the inner pipe drags the fluid near the wall, more fluids seek to flow through zones of least resistance (sector C-C), thus, increasing the peak velocity profile in sector C-C. As similar to concentric annulus, it shows that as the axial velocity increases, more fluid near the inner pipe boundary is dragged in a downward motion. In sector C-C, as the inner pipe tripping velocity increases, the yielded plug flow region decreases. This is because as the tripping speed increases, the fluid near the inner pipe become more shear thinning compare to the fluid at the centre annulus (low-sheared region), therefore, the fluid can be dragged by the inner pipe easily. This phenomena also gives indication of effect of dynamic viscosity on the axial flow profiles. The justification about the relation of dynamic viscosity will be further explain in section 4.2.4. Furthermore, as a comparison of the same shear thinning fluid ($n < 1$), it shows that fluid 0.75% PAC-B yield greater plug region than fluid 1.00% PAC-B. This is because as the fluid's flow behaviour ($n$) is shear thinning, the consistency index of the fluid becomes more dominant. It is observed that as the consistency index is higher, the shear rate increases, the dynamic viscosity decreases and subsequently decreases the yielded plug flow region. In addition, as similar observation made by Ofei et al [12], the flow behaviour in both narrow and wide regions indicates that the narrower the annular gap, the better the shearing rate. As similar to concentric annulus, the axial velocity gradient increases with increasing inner pipe tripping velocity. On the other hand, the peak axial velocity of fluid 0.75% PAC-B is lower than the fluid 1.00% PAC-B.

As comparison of the effect of eccentricity on the axial velocity pattern, higher eccentricity generates more yielded plug flow region than lower eccentricity. Hence, the cuttings transport and hole cleaning in eccentric annulus is better than the concentric annulus.

### 4.2.4 Dynamic viscosity

All the test fluids in this study exhibits a shear thinning behaviour. The analysis on axial velocity profiles have found a relation between velocity profile and shear rate, and consequently, shear rate is related to the dynamic viscosity. The dynamic viscosity results for concentric and eccentric annulus are presented as follow:

v=0.8 ft/s

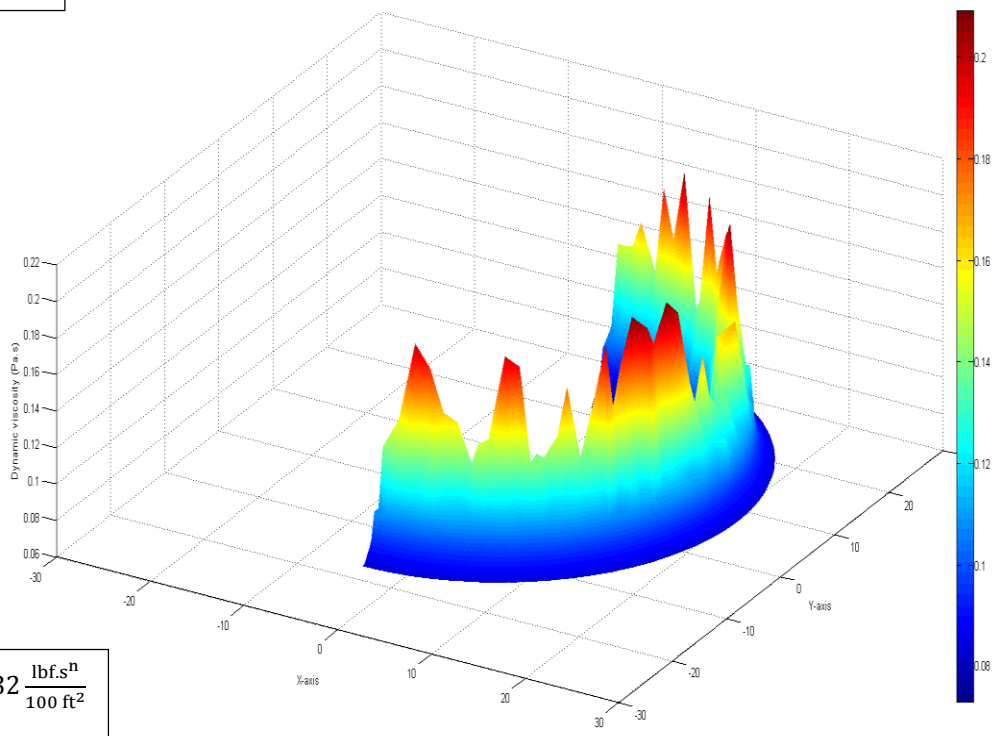


$K=0.532\ \frac{\text{lbf.s}^n}{100\ \text{ft}^2}$

n=0.781

Figure 4-13. Dynamic viscosity of 0.75% PAC-A

v=0.8 ft/s

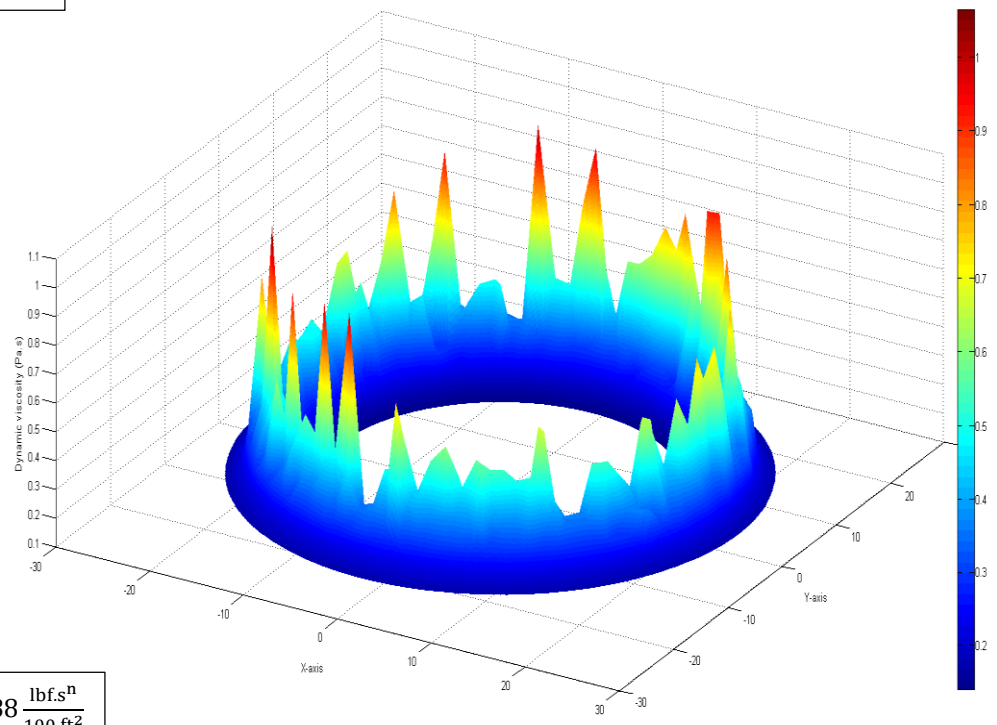


$K=2.188\ \frac{\text{lbf.s}^n}{100\ \text{ft}^2}$

n=0.652

Figure 4-14. Dynamic viscosity of 1.00% PAC-A

In concentric annulus, the dynamic viscosity of 0.75% PAC-A fluid is lower than 1.00% PAC-A fluid. However, for both fluids, the peak of the fluid dynamic viscosity is located at the central area of the annulus and decreases when the dynamic viscosity is near to the wall boundary. This indicates that the centre area of annulus is a low-sheared region and has higher dynamic viscosity, meanwhile, a steep velocity profile near the walls is an indication of high shearing (lower viscosity). This totally shows the behaviour of the shear thinning fluid.

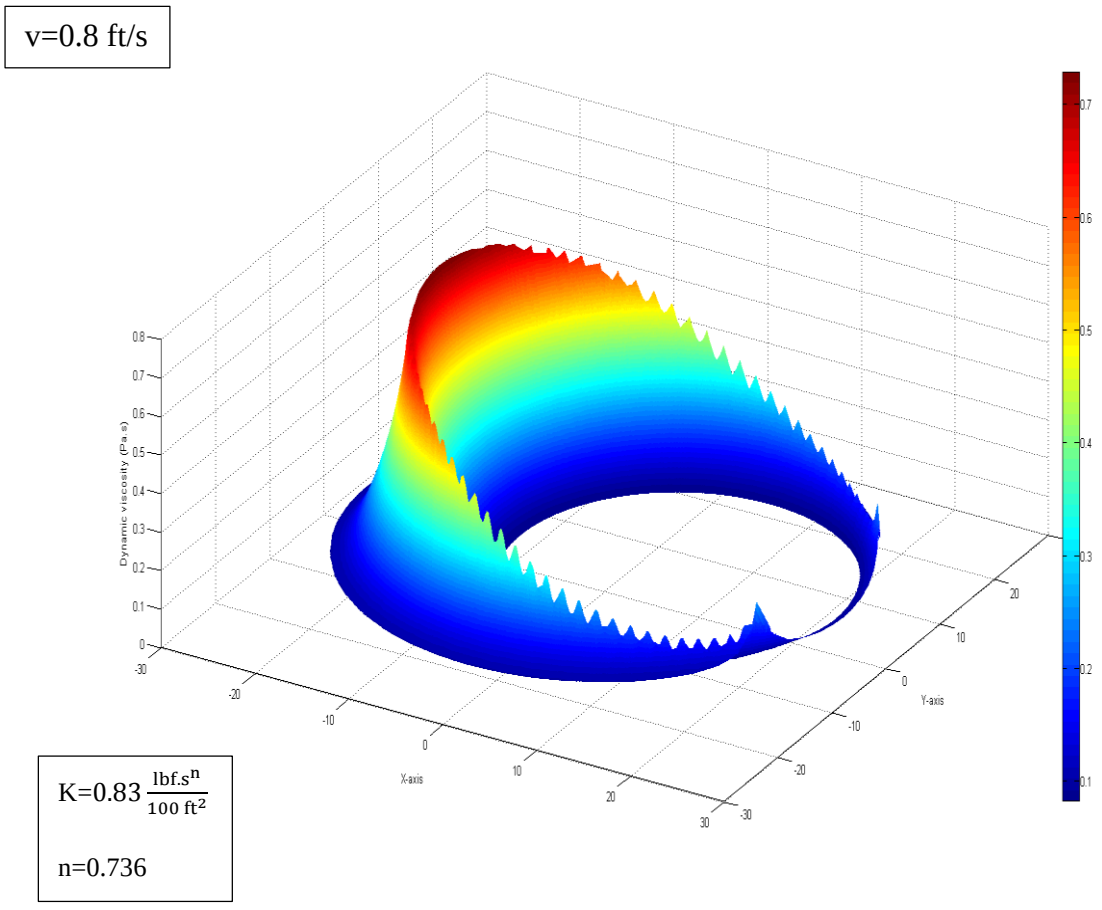


Figure 4-15. Dynamic viscosity of 0.75% PAC-B

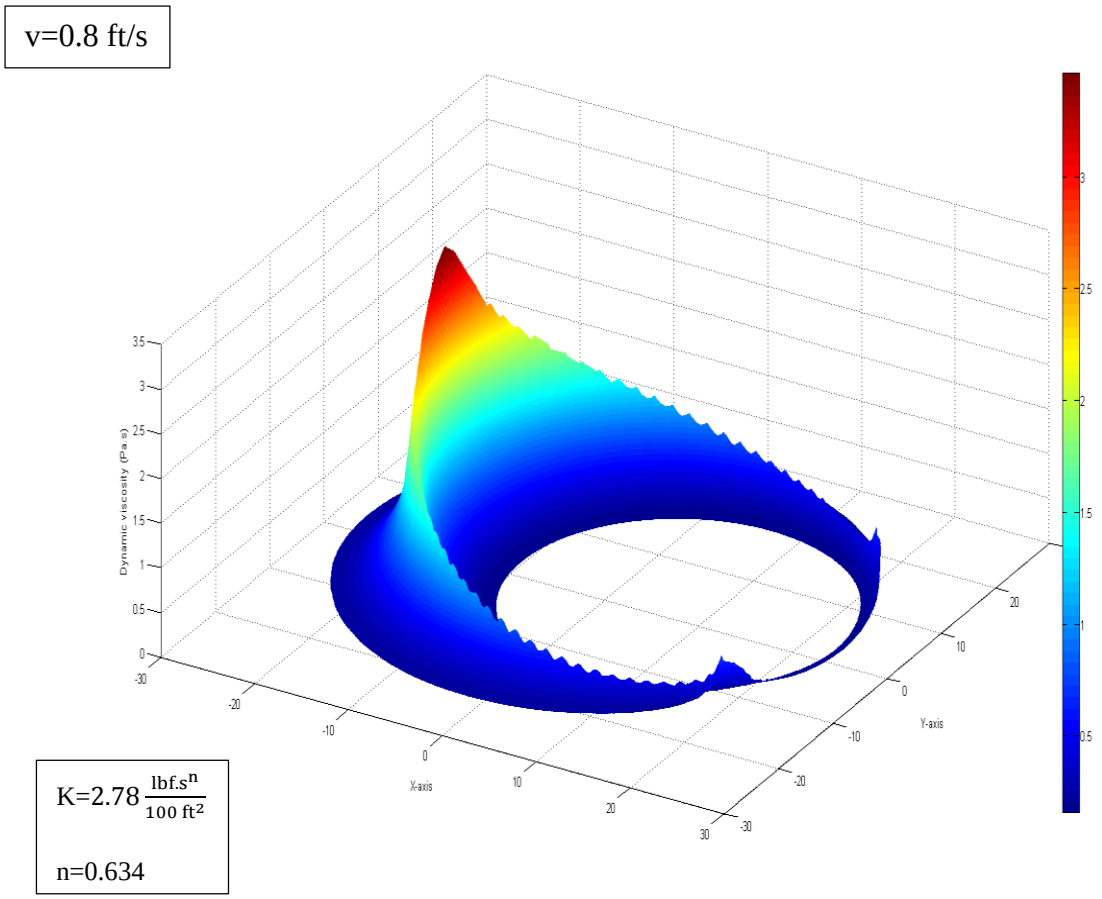


Figure 4-16. Dynamic viscosity of 1.00% PAC-B

For eccentric annulus, at the narrow region (sector B-B), the dynamic viscosity for both fluid is nearly zero. This indicates that the fluid at the narrow region is completely sheared by the downward movement of the inner pipe and stationary outer pipe movement. No positive flow is observed at the narrow region as the fluid is dragged by the inner pipe that overcomes the shear stress of the fluid. The dynamic viscosity shows more significant difference in wide region (sector C-C). As mention earlier from section 4.2.3, the yielded plug flow region at the centre area of the annulus is the low-sheared region for both of fluid 0.75% PAC-B and 1.00% PAC-B. This shows strong agreement with Ofei et al [12], as from the study, it is showed that the higher dynamic viscosity is located at the centre region of the annulus for both fluid. This strongly agrees that the higher dynamic viscosity relates to the lower sheared velocity in the mid annulus [12]. The results show that as for similar shear thinning fluid, the shear rate decreases with increasing dynamic viscosity, thus the axial flow profile is higher.

# CHAPTER 5
# CONCLUSION AND RECOMMENDATION

A CFD simulation has been carried out to predict surge/swab pressures in both concentric and eccentric annuli flowing with Power-law fluid. The effects of pipe tripping velocity and eccentricity were considered in this study. Based on the work performed, the following conclusion can be made:

- The simulation model was validated against experimental surge pressure data with very good agreement (the highest MPE is 14.3%), thus, confirming the validity of the current model setup. This can conclude that the CFD simulation reasonably predict the surge pressure gradient.
- The narrow slot model correlation from Crespo and Ahmed [3], totally under predict the experimental surge pressure with highest mean percentage error (MPE) of 96.9%.
- The degree of eccentricity has substantial effects in the surge and swab pressure. It has been determined that the effect of eccentricity by 0.9 reduced the surge pressure gradient by 18%. In addition, it is found that as the inner pipe tripping velocity increases, the rate of surge pressure reduction increases.
- Based on the velocity profile analysis, as the axial velocity increases, more fluid near the inner pipe boundary is dragged in a downward motion. Furthermore, it is showed that when the inner pipe tripping velocity increases, the yielded plug flow region decreases.
- According to dynamic viscosity analysis, it is strongly agreed with Ofei et al [12], the higher dynamic viscosity relates to the lower sheared velocity in the mid annulus. Moreover, the centre of the annulus generates higher dynamic viscosity and decreases as it approach the inner and outer pipe wall.

As a recommendation, the combined effect of drillpipe rotation and axial motion should be examined to observe their effect on surge pressure and annular flow pattern. Cuttings can also be introduced into the fluid domain to analyse how the combined effect of pipe rotation and axial motion will effect cuttings removal and annular pressure loss. Furthermore, introduction

the cuttings also can alter the fluid density, thus, the effect of the surge pressure can be monitored.

In addition, it is recommend that the surge pressure gradient prediction is scale up to the real field environment. The experimental study and CFD simulation are performed based on the experimental scale. The action to scale up the experimental condition to a real field condition can provide the industry on the better understanding and prediction of the surge pressure gradient on the real field condition. Moreover, since the CFD simulation model has been developed, it is recommended to develop a set of empirical equation from the CFD simulation correlation in predicting the surge pressure.

Last but not least, this study considers vertical well. Deviated and horizontal wells can be modelled to study the effects of well trajectory on annular flow profile and surge pressure gradient.

# REFERENCES


[1] R. Srivastav, "Experimental study and modeling of surge and swab pressures in eccentric annulus," Norman, Oklahoma, 2013.

[2] R. Srivastav, M. Enfis, F. Crespo, R. Ahmed and A. Saasen, "Surge and Swab Pressures in Horizontal and Inclined Wells," in *SPE Latin American and Carribbean Petroleum Engineering Conference*, Mexico City, Mexico, 2012.

[3] F. Crespo and R. Ahmed, "A simplified surge and swab pressure model for yield power law fluids," *Journal of Petroleum Science and Engineering*, vol. 101, pp. 12-2-, January 2013.

[4] R. K. Clark and J. E. Fontenot, *Field Measurements of the Effects of Drillstring Velocity, Pump Speed, and Lost Circulation Material on Downhole Pressures*, Houston: Society of Petroleum Engineers, 1974.

[5] P. L. Moore, "Pressure Surges and their Effect on Hole Conditions," *Oil and Gas Journal*, p. 90, 13 December 1965.

[6] "Oilfield Glosarry," Schlumberger , December 2014. [Online].

[7] A. T. Bourgoyne Jr., K. K. Millheim, M. E. Chenevert and F. Young Jr., Applied Drilling Engineering, vol. 1, Richardson, TX: SPE Textbook Series, 1986.

[8] P. L. Moore, Drilling Practice Manual, Tulsa: Petroleum Publishing Co., 1974, pp. 241-252.

[9] Q. E. Hussain and M. A. R. Sharif, "Viscoplastic Fluid Flow in Irregular Eccentric Annuli Due to Axial Motion of the Inner Pipe," *The Canadian Journal of Chemical Engineering*, vol. 75, no. 6, pp. 1038-1045, 1997.

[10] A. P. Singh and R. Samuel, *Effect of Eccentricity and Rotation on Annular Frictional Pressure Losses With Standoff Devices*, New Orleans: Society of Petroleum Engineers, 2009.

[11] M. Zamora and D. Jefferson, “Flow Visualization of Solids Transport by Drilling Fluids in Inclined Wells,” *Developments in Non-Newtonian Flows*, vol. 175, pp. 115-130, 1993.

[12] T. N. Ofei, S. Irawan, W. Pao and R. E. Osgouei, “Modified yield power-law fluid flow in narrow annuli with inner rotating pipe,” *The canadian journal of chemical engineering*, vol. 93, January 2015.

[13] C. A. Shook and M. C. Roco, Slurry Flow: Principles and Practice, London: Butterworth-Heimemann, 1991.

[14] W. M. Rohsenow, J. P. Hartnett and Y. I. Cho, Handbook of heat transfer, McGraw-Hill Professional, 1998.

[15] M. Aftosmis, D. Gaitonde and T. S. Tavares, “On the accuracy, stability, and mono tonicity of various reconstruction algorithms for instructured meshes,” in *32nd AIAA Aerospace Science Meeting*, 1994.

# APPENDIX

## APPENDIX A

ECCENTRIC EDGE SIZING

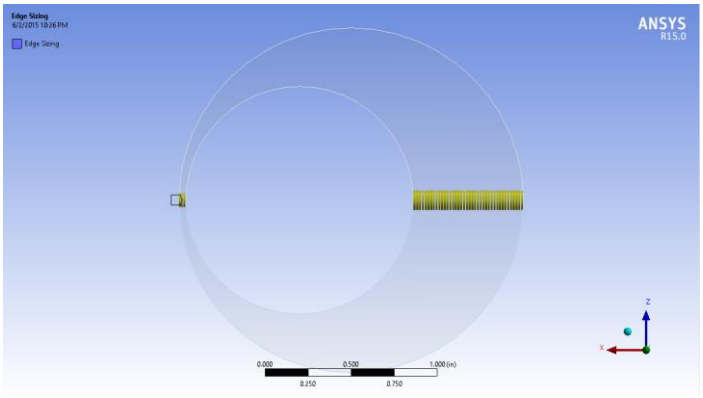


Figure 0-1. Radius edge no. of division ($r$).

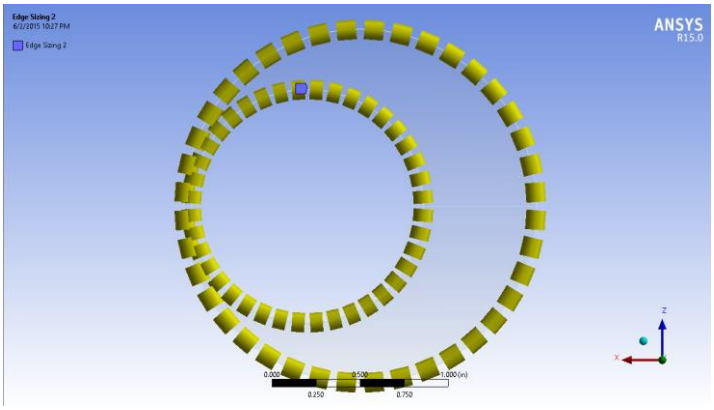


Figure 0-2. Circumference edge no. of division ($\theta$).

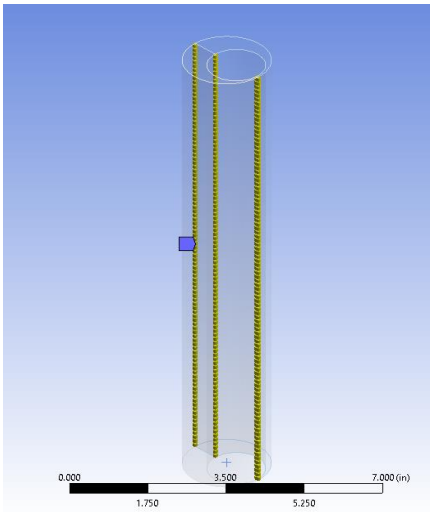


Figure 0-3. Length edge no. of division ($z$).

**APPENDIX B**

CONCENTRIC EXPERIMENTAL AND CFD SIMULATION RESULTS

Table 0-1. Concentric surge pressure measurement: 1.00% PAC-A

| 1.00% PAC-A | | | |
|---|---|---|---|
| Tripping velocity (ft/s) | Experimental [1] | CFD Simulations | Percentage of error (%) |
| | Surge Pressure gradient (psi/ft) | | |
| 0.1 | 0.1115 | 0.0990 | 11.21 |
| 0.2 | 0.1757 | 0.1556 | 11.42 |
| 0.3 | 0.2362 | 0.2028 | 14.13 |
| 0.4 | 0.2601 | 0.2448 | 5.89 |
| 0.5 | 0.285 | 0.2833 | 0.61 |
| 0.6 | 0.3141 | 0.3192 | 1.62 |
| 0.7 | 0.3321 | 0.3531 | 6.32 |
| 0.8 | 0.3506 | 0.3854 | 9.93 |
| Mean percentage error (%) | | | 7.64 |

Table 0-2. Concentric surge pressure measurement: 0.75% PAC-A

| 0.75% PAC-A | | | |
|---|---|---|---|
| Tripping velocity (ft/s) | Experimental [1] | CFD Simulations | Percentage of error (%) |
| | Surge Pressure gradient (psi/ft) | | |
| 0.1 | 0.0523 | 0.0352 | 32.75 |
| 0.2 | 0.0757 | 0.0605 | 20.02 |
| 0.3 | 0.0933 | 0.0832 | 10.81 |
| 0.4 | 0.1172 | 0.1045 | 10.87 |
| 0.5 | 0.1505 | 0.1246 | 17.24 |
| 0.6 | 0.1684 | 0.1438 | 14.59 |
| 0.7 | 0.1833 | 0.1625 | 11.37 |
| 0.8 | 0.2037 | 0.1807 | 11.31 |
| Mean percentage error (%) | | | 16.12 |

ECCENTRIC EXPERIMENTAL AND CFD SIMULATION RESULTS

Table 0-3. Eccentric surge pressure measurement: 1.00% PAC-B

| 1.00% PAC-B | | | |
|---|---|---|---|
| Tripping velocity (ft/s) | Experimental [1] | CFD Simulations | Percentage of error (%) |
| | Surge Pressure gradient (psi/ft) | | |
| 0.1 | 0.0888 | 0.0755 | 14.93 |
| 0.2 | 0.1391 | 0.1238 | 11.01 |
| 0.3 | 0.1742 | 0.1657 | 4.87 |
| 0.4 | 0.2087 | 0.2041 | 2.18 |
| 0.5 | 0.2459 | 0.2409 | 2.04 |
| 0.6 | 0.2785 | 0.2761 | 0.85 |
| 0.7 | 0.2989 | 0.3093 | 3.47 |
| 0.8 | 0.3271 | 0.3411 | 4.28 |
| Mean percentage error (%) | | | 5.46 |

Table 0-4. Eccentric surge pressure measurement: 0.75% PAC-B

| 0.75% PAC-B | | | |
|---|---|---|---|
| Tripping velocity (ft/s) | Experimental [1] | CFD Simulations | Percentage of error (%) |
| | Surge Pressure gradient (psi/ft) | | |
| 0.1 | 0.0306 | 0.0383 | 25.03 |
| 0.2 | 0.053 | 0.0675 | 27.44 |
| 0.3 | 0.0836 | 0.0942 | 12.63 |
| 0.4 | 0.1011 | 0.1197 | 18.41 |
| 0.5 | 0.1202 | 0.1445 | 20.18 |
| 0.6 | 0.1322 | 0.1681 | 27.13 |
| 0.7 | 0.1487 | 0.1873 | 25.99 |
| 0.8 | 0.162 | 0.2091 | 29.10 |
| Mean percentage error (%) | | | 23.24 |

**APPENDIX C**

EFFECT OF ECCENTRICITY

Table 0-5. Surge pressure measurement for different eccentricity

| Tripping velocity (ft/s) | Difference of Surge Pressure gradient (%) |
|---|---|
| 0.1 | 10.81 |
| 0.2 | 14.67 |
| 0.3 | 17.10 |
| 0.4 | 18.72 |
| 0.5 | 19.52 |
| 0.6 | 19.83 |
| 0.7 | 20.19 |
| 0.8 | 20.42 |
| Average surge pressure difference (%) | 17.66 |

**APPENDIX D**

Table 0-6. Project Gantt Chart and key milestone

| No. | Activities/Weeks | 1 | 2 | 3 | 4 | 5 | 6 | 7 | 8 | 9 | 10 | 11 | 12 | 13 | 14 |
|---|---|---|---|---|---|---|---|---|---|---|---|---|---|---|---|
| 1 | Literature review | | | | | | | | | | | | | | |
| 2 | Model design using ANSYS Workbench | | | | | | | | | | | | | | |
| 3 | Model meshing and grid independent study | | | | | | | | | | | | | | **1** |
| **No.** | **Activities/Weeks** | **15** | **16** | **17** | **18** | **19** | **20** | **21** | **22** | **23** | **24** | **25** | **26** | **27** | **28** |
| 1 | Model validation and simulation run | | | | | | | | | | **2** | | | | |
| 2 | Analysis of simulation data: surge pressures and annular flow pattern | | | | | | | | | | | | **3** | | |
| 3 | Report writing and viva voce | | | | | | | | | | | | | | |

| | | |
|---|---|---|
| **1** | **Model design, mesh optimization and Grid Independence study** | **Week 14** |
| **2** | **Model validation and simulation run** | **Week 24** |
| **3** | **Data analysis** | **Week 26** |